Particle Accelerators, 1990, Vol. 25, pp. 113–151
Reprints available directly from the publisher
Photocopying permitted by license only

Printed in the United States of America

FIELDS EXCITED BY A BEAM IN A SMOOTH TOROIDAL CHAMBER†

R. L. WARNOCK and P. MORTON
Stanford Linear Accelerator Center, Stanford University, Stanford, California 94309

(Received March 8, 1988)

We study the fields produced by a beam circulating in a smooth toroidal chamber with walls of finite conductivity. At high frequencies the beam can excite resonant modes of the chamber having phase velocity equal to the particle velocity. The frequencies of these synchronous modes are widely spaced and depend sensitively on the revolution frequency ω_0. The associated longitudinal coupling impedance, $Z(n, n\omega_0)$, has relatively broad peaks as a function of the azimuthal mode number n. In typical cases $\mathrm{Re}\, Z(n, n\omega_0)/n$ reaches values of several ohms in the lowest modes. The lowest mode has n somewhat greater than $\pi R^{3/2}/w^{1/2}h$, where R is the trajectory radius, and the cross section of the chamber is a rectangle of width w and height h. Although the frequencies are typically quite high, it is not excluded that the large coupling impedance could lead to fast microwave instabilities of a short bunch.

1. INTRODUCTION

We discuss the fields produced by an arbitrary particle beam following a circular trajectory inside a toroidal vacuum chamber. The torus has a rectangular cross section, as shown in Fig. 1, and the walls have finite conductivity. Our interest in this problem stems from a general concern about the sources of beam coupling impedance at high frequencies, well beyond the beam-tube cutoff. The trend toward shorter particle bunches in storage rings and linacs encourages such concern.

It has long been known that classical synchrotron radiation, shielded by conducting surfaces, would entail a large self-force on the beam at sufficiently high frequencies. Several models led to quantitative results, for instance a system of two parallel plates with circular beam orbit in a plane midway between the plates. In this model, the self-force leads to energy loss characterized by a coupling impedance $Z(n, \omega)$ such that

$$\left.\frac{\mathrm{Re}\, Z(n, n\omega_0)}{n}\right|_{\max} \approx 300 \frac{g}{R}\,\Omega, \tag{1}$$

where the distance between the plates is $2g$, and R is the orbit radius. Here n is

† Work supported by the Department of Energy, contract DE-AC03-76SF00515.

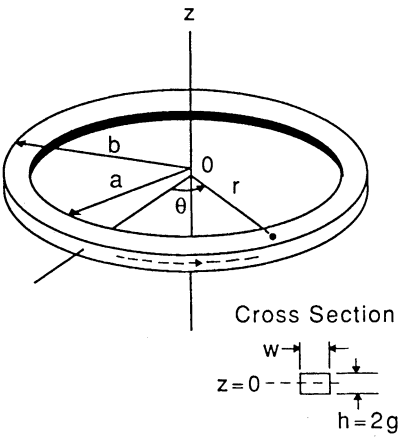

FIGURE 1 Toroidal vacuum chamber with cylindrical cross section of width w and height $h = 2g$. The inner (outer) torus radius is a (b). The origin for cylindrical coordinates is at the midplane of the torus.

the azimuthal mode number, and $\omega_0 = \beta c/R$ is the revolution frequency. The value of n at which Re Z/n achieves the maximum of Eq. (1) is roughly $(R/g)^{3/2}$.

The open structure of two parallel plates allows radiation of energy to infinity. The analogous phenomenon in the closed toroidal structure is radiation into resonant modes of the chamber. If the walls have infinite conductivity, the energy remains forever in the resonant field mode; otherwise it is dissipated in wall heating. Nonresonant loss of beam energy is usually negligible by comparison, being of the same magnitude as the usual resistive-wall effect in a straight beam tube; hence, it is zero for infinite conductivity. The frequency of the first resonance in $Z(n, n\omega_0)$ is comparable to the frequency of maximum radiation for the open parallel-plate system. For typical wall materials, the peak toroidal values of Re Z/n exceed substantially the parallel-plate value [Eq. (1)].

For the lowest resonant mode the dispersion relation of the toroidal structure is approximated closely at large n by

$$\omega(n) = \frac{c}{b}\left[\left(\frac{\pi p b}{h}\right)^2 + n^2 + \left(\frac{3\pi}{4}\right)^{2/3} n^{4/3}\right]^{1/2}, \tag{2}$$

where b is the outer radius and h is the height of the chamber, as defined in Fig. 1. The synchronism condition, the requirement that the phase velocity of the longitudinal field be equal to the particle velocity, is $\omega_0 n = \beta c n/R$. For a synchronous mode to exist at some n, the asymptotic slope of the curve $\omega(n)$, which is c/b, must be less than the slope of the line $\omega = \omega_0 n$, so that the curve and the line may intersect. Thus,

$$\beta \frac{b}{R} > 1. \tag{3}$$

Typically the curve $\omega(n)$ and the line $\omega = \omega_0 n$ intersect at a very small angle, so

that n at the point of intersection is a sensitive function of ω_0. The synchronous resonant frequency is therefore a sensitive function of the orbit radius R. A related circumstance is that resonance peaks in $Z(n, n\omega_0)$, the latter regarded as a function of n, are much broader than the natural line width of the resonance. When n changes by one unit, $\omega(n)$ changes by an amount $d\omega/dn \approx c/b$ that is close to ω_0. Therefore, $Z(n+1, [n+1]\omega_0)$ is close to $Z(n, n\omega_0)$; the peak is thereby broadened.

Because of the peculiar features of the impedance, we defer any comments on the implications of our results for beam stability. We do not recommend an uncritical application of conventional formulas for the threshold of instability. A re-examination of the Vlasov analysis of bunched beam stability seems appropriate in the present case.

Since the theory of classical synchrotron radiation has evolved over many years, there are numerous points of contact between our work and earlier efforts.[1–18] Schwinger[2] and Schiff[3] discussed shielded coherent radiation in 1945 and 1946. Neil[8] treated our problem in his Ph.D. thesis, and made further studies in collaboration with Judd, Laslett, and Sessler.[8] Laslett and Lewish[9] studied relevant properties of Bessel functions and stated formulas for the quality factor of a toroidal chamber. Faltens and Laslett[13] and J. Bisognano (private communication) did much to encourage our work by emphasizing the result from Eq. (1) and its probable general import. Bart's technique[15] for treating planar resistive walls was essential to our results. L. Smith (unpublished notes, 1985) sketched a treatment of the toroidal chamber, using methods similar to those of Neil. Recent work[16–20] on the transverse self-force of particles in curved orbits involves some of the same calculations that we have pursued. After this work was completed, we learned of a recent analysis of our problem by K.-Y. Ng (Ref. 24). Also, one of the authors and Ng extended the present treatment to obtain the reactive impedance at all frequencies up to the lowest resonance (Ref. 25).

Of the various works, those of Neil *et al.* and Ng are most similar to ours in scope. We use different techniques at several points, usually chosen for mathematical clarity, and discuss some physical points and parameter ranges not covered in the other papers. Most of the previous discussions have been based on an expansion in eigenfunctions of the structure. We prefer a Fourier–Bessel expansion which does not employ eigenfunctions. This expansion, which appears along with the eigenfunction development in Neil's thesis, leads to a relatively transparent formula for the impedance and is much easier to evaluate in nonresonant regions. Near a resonance, the two expansions lead to roughly the same calculations. We also differ from other authors in the treatment of wall resistance. All other authors have treated wall resistance perturbatively, by integrating an approximate expression for the Poynting vector over the metallic surfaces. This yields definite formulas for the quality factor Q, but gives no information about the importance of higher-order effects. We prefer to solve the field equations subject to the resistive-wall boundary condition, so as to incorporate the higher-order effects completely. This method reveals shortcomings in the treatment of planar walls (top and bottom of the chamber) that are not apparent in the usual treatment. Our formulation shows how to overcome the

difficulties through a coupled-mode treatment, but we have not carried the computation that far in the present work.

The case of a beam circulating in a cylindrical "pillbox" chamber is similar to the toroidal case in most important respects, but somewhat easier to analyze. To make our story simple we first treat the cylindrical problem, in Section 2, and then give the obvious generalizations to handle the torus, in Section 3. Sections 2 and 3 end with formulas for the longitudinal coupling impedance in terms of Bessel functions. In Section 4 we evaluate the impedance at low frequency, finding a very small value. In Section 5 we employ appropriate asymptotic expansions of Bessel functions to locate resonance poles at high frequencies and to find the pole residues that determine R/Q. We find a rather accurate explicit formula for the frequency of synchronous resonant modes. If the beam is not too close to the inner wall of the torus, the results for the pillbox and torus are nearly identical.

For studies of beam stability, it is important to account for the resistance of the vacuum-chamber walls. In Section 6 we give a treatment of wall resistance that is valid close to the resonances. At frequencies away from the resonances, it is difficult to include resistance on the planar walls (top and bottom). Since our impedance is dominated by the resonances, this is not a great drawback.

In Section 7 we give numerical results for the impedance of the toroidal chamber with wall resistance and try to explain peculiar features of the impedance in terms of the dispersion relation.

Our notation for special functions follows Ref. 21, Abramowitz and Stegun. We refer to equation numbers in that book following this example: A.–S. 9.3.35.

We hope to treat beam stability and transverse impedances in later papers.

2. FIELDS AND LONGITUDINAL COUPLING IMPEDANCE FOR A CYLINDRICAL CHAMBER

In this section, we find expressions for the fields produced by a beam circulating in a cylindrical pillbox chamber, assuming that the wall conductivity is infinite. In solving this preliminary problem we set down the definitions and apparatus required for the rest of the work and provide a useful way of viewing the full problem of the torus.

We put $a = 0$ (see Fig. 1) to obtain a cylindrical chamber of radius b and height $h = 2g$. We use cylindrical coordinates (r, θ, z) with the z-axis along the symmetry axis of the cylinder and with the origin at the centroid of the chamber; thus the plane surfaces are at $z = \pm g$. We use mks units and adopt the usual definition of Z_0, the "impedance of free space":

$$Z_0 = \left(\frac{\mu_0}{\epsilon_0}\right)^{1/2} = \mu_0 c = \frac{1}{\epsilon_0 c} = 120\,\pi\Omega. \tag{4}$$

We shall first express the fields produced by an arbitrary charge-current distribution and then specialize for the particle beam of interest. All components of the fields can be expressed in terms of Fourier amplitudes of H_z and E_z.

Accordingly, we begin with the Fourier expansions,

$$H_z(r, \theta, z, t) = \int_{-\infty}^{\infty} d\omega e^{-i\omega t} \sum_{n=-\infty}^{\infty} e^{in\theta} \sum_{p=1}^{\infty} \sin \alpha_p(z+g) H_{znp}(r, \omega), \tag{5}$$

$$E_z(r, \theta, z, t) = \int_{-\infty}^{\infty} d\omega e^{-i\omega t} \sum_{n=-\infty}^{\infty} e^{in\theta} \sum_{p=0}^{\infty} \cos \alpha_p(z+g) E_{znp}(r, \omega), \tag{6}$$

where the wave number for the z-direction is

$$\alpha_p = \frac{\pi p}{2g}. \tag{7}$$

The other components will have similar expansions. In each component the z-dependent factor is either $\sin \alpha_p(z+g)$ or $\cos \alpha_p(z+g)$, chosen according to the following scheme:

$$(E_r, H_\theta, H_r, E_\theta) \leftrightarrow (\sin, \cos, \cos, \sin). \tag{8}$$

The forms of H_z, E_r, and E_θ were chosen to meet the boundary conditions

$$H_z = 0, \qquad E_r = E_\theta = 0, \qquad z = \pm g, \tag{9}$$

term by term in the Fourier developments. The forms of the other fields were selected so that the source-free Maxwell equations would also be satisfied term-by-term. For a consistent term-by-term satisfaction of the Maxwell equations with sources, we must also expand the current and charge in Fourier series, with z-dependent factor $\sin \alpha_p(z+g)$ or $\cos \alpha_p(z+g)$ chosen as follows:

$$(J_r, J_\theta, J_z, \rho) \leftrightarrow (\sin, \sin, \cos, \sin). \tag{10}$$

One might ask whether our Fourier series in z actually represent general solutions of Maxwell's equations, since one usually expects both sines and cosines to be present in a generally valid expansion. By considering an artificial odd or even extension of each field to an interval of twice the length h, one can show that the expansions are indeed general.

After substituting the series in Maxwell's equations, and taking Fourier transforms with respect to t, θ, and z, one gets a set of equations for the r-dependent Fourier amplitudes. The equations may be solved algebraically to express all amplitudes in terms of H_{znp} and E_{znp}. The calculation yields

$$E_{rnp} = \frac{-1}{\gamma_p^2}\left[\alpha_p \frac{\partial E_{znp}}{\partial r} + \frac{\omega}{c} Z_0\left(\frac{n}{r} H_{znp} + iJ_{rnp}\right)\right], \tag{11}$$

$$H_{\theta np} = \frac{i}{\gamma_p^2}\left[\frac{\omega}{c}\frac{1}{Z_0}\frac{\partial E_{znp}}{\partial r} + \alpha_p\left(\frac{n}{r} H_{znp} + iJ_{rnp}\right)\right], \tag{12}$$

$$H_{rnp} = \frac{1}{\gamma^2}\left[\frac{\omega}{c}\frac{1}{Z_0}\frac{n}{r} E_{znp} + \alpha_p\left(\frac{\partial H_{znp}}{\partial r} + J_{\theta np}\right)\right], \tag{13}$$

$$E_{\theta np} = \frac{-i}{\gamma_p^2}\left[\alpha_p \frac{n}{r} E_{znp} + \frac{\omega}{c} Z_0\left(\frac{\partial H_{znp}}{\partial r} + J_{\theta np}\right)\right], \tag{14}$$

where the "radial wave number," γ_p, is defined by

$$\gamma_p^2 = \left(\frac{\omega}{c}\right)^2 - \alpha_p^2. \tag{15}$$

Here, and in much of the following, we use abbreviated notation in which the dependence of amplitudes on r and ω is not indicated. Maxwell's equations also imply the radial wave equations, which serve to determine H_{znp} and E_{znp}:

$$\frac{1}{r}\frac{\partial}{\partial r}\left(r\frac{\partial H_{znp}}{\partial r}\right) + \left(\gamma_p^2 - \frac{n^2}{r^2}\right)H_{znp} = -\frac{1}{r}\frac{\partial}{\partial r}(rJ_{\theta np}) + i\frac{n}{r}J_{rnp}, \tag{16}$$

$$\frac{1}{r}\frac{\partial}{\partial r}\left(r\frac{\partial E_{znp}}{\partial r}\right) + \left(\gamma_p^2 - \frac{n^2}{r^2}\right)E_{znp} = Z_0\left(-i\frac{\omega}{c}J_{znp} + \alpha_p c\rho_{np}\right). \tag{17}$$

When the sources J, ρ are zero, the general solution of Eq. (16) or (17) is a linear combination of $J_n(\gamma_p r)$ and $Y_n(\gamma_p r)$, linearly independent Bessel functions. Equivalently, it is a linear combination of $I_n(\Gamma_p r)$ and $K_n(\Gamma_p r)$, the modified Bessel functions, where

$$\Gamma_p^2 = -\gamma_p^2 = \alpha_p^2 - \left(\frac{\omega}{c}\right)^2. \tag{18}$$

It is convenient to use the former representation when $\gamma_p^2 > 0$ and the latter when $\Gamma_p^2 > 0$, so that we always deal with functions of real argument. Since our discussion emphasizes resonances, for which $\gamma_p^2 > 0$, we give our general formulas in terms of J_n, Y_n and provide some translations to the I_n, K_n basis where appropriate.

In the presence of sources, the general solution is the sum of the general solution of the source-free equation and any particular solution of the equation with sources. Thus we may write the general solutions of Eqs. (16) and (17) as

$$E_{znp}(r) = A_{np}J_n(\gamma_p r) + B_{np}Y_n(\gamma_p r) + e_{znp}(r), \tag{19}$$

$$H_{znp}(r) = C_{np}J_n(\gamma_p r) + D_{np}Y_n(\gamma_p r) + h_{znp}(r), \tag{20}$$

where e_z and h_z are particular solutions of the inhomogeneous equations.

In the present pillbox problem, the solutions Eqs. (19) and (20) must be bounded at $r = 0$. Let us choose e_z and h_z so that $e_{znp}(0) = 0$, $h_{znp}(0) = 0$; we shall see how to do this presently. With that choice we must have $B_{np} = D_{np} = 0$, since $Y_n(\gamma_p r)$ is unbounded at $r = 0$. In the torus problem, the Y_n term is allowed and necessary.

Particular solutions of the inhomogeneous equations are derived easily by the method of variation of parameters (equivalently, by finding the Green function of the Bessel differential operator). A calculation yields

$$e_{znp}(r) = -\frac{\pi}{2}\left[J_n(\gamma_p r)\int_a^r u\,du\,Y_n(\gamma_p u) - Y_n(\gamma_p r)\int_a^r u\,du\,J_n(\gamma_p u)\right]$$
$$\times Z_0\left[-i\frac{\omega}{c}J_{znp}(u) + \alpha_p c\rho_{np}(u)\right], \tag{21}$$

$$h_{znp}(r) = -\frac{\pi}{2}\left[J_n(\gamma_p r)\int_a^r u\,du\,Y_n(\gamma_p u) - Y_n(\gamma_p r)\int_a^r u\,du\,J_n(\gamma_p u)\right]$$
$$\times\left[-\frac{1}{u}\frac{\partial}{\partial u}[uJ_{\theta np}(u)] + i\frac{n}{u}J_{rnp}(u)\right]. \tag{22}$$

It is easy to check that these are indeed solutions, if one recalls the value of the Wronskian,

$$W(J_n, Y_n) = J_n(x)Y_n'(x) - Y_n(x)J_n'(x) = \frac{2}{\pi x}. \tag{23}$$

We choose the lower limit, a, so that all charges are located at points with $r > a$, and $a > 0$. In the work of Section 3, a will be the inner torus radius. Now for $r = 0$ the integrals in Eqs. (21) and (22) will not encompass any points where charge or current is nonzero, and $e_{znp}(0) = 0$, $h_{znp}(0) = 0$, as promised above.

In addition to the boundary conditions [Eq. (9)] on the planar surfaces, we have conditions on the cylindrical surfaces,

$$H_r = 0, \qquad E_z = E_\theta = 0, \qquad r = b. \tag{24}$$

Referring to Eqs. (13) and (14), we see that these conditions will be met if

$$E_{znp}(b) = 0, \qquad \frac{\partial H_{znp}}{\partial r}(b) = 0. \tag{25}$$

Now Eq. (25) determines A_{np}, C_{np} in Eqs. (19) and (20), since $B_{np} = D_{np} = 0$. Thus the determination of E_{znp} and H_{znp} is complete:

$$E_{znp}(r) = -\frac{J_n(\gamma_p r)}{J_n(\gamma_p b)}e_{znp}(b) + e_{znp}(r), \tag{26}$$

$$H_{znp}(r) = -\frac{J_n(\gamma_p r)}{\gamma_p J_n'(\gamma_p b)}h_{znp}'(b) + h_{znp}(r), \tag{27}$$

where primes denote derivatives.

Having found the solution for general sources, we now take a particular source to compute the longitudinal coupling impedance. We describe a rigid bunch of particles with total charge q, following a circular trajectory of radius R in the median plane of the chamber, $z = 0$, and having angular revolution frequency

$$\omega_0 = \frac{\beta c}{R}. \tag{28}$$

The charge density is taken to be

$$\rho(r, \theta, z, t) = q\lambda(\theta - \omega_0 t)H(z)W(r), \tag{29}$$

where $\lambda(\theta + 2\pi) = \lambda(\theta)$, and $H(z)$ and $W(r)$ are concentrated near $z = 0$ and $r = R$, respectively. The corresponding current, which with Eq. (29) satisfies the continuity equation, is

$$(J_r, J_\theta, J_z) = (0, \beta c\rho r/R, 0). \tag{30}$$

The functions in Eq. (29) are normalized so that

$$\int_0^{2\pi} \lambda(\theta)\, d\theta = 1, \int_{-g}^{g} dz H(z) = 1, \int_a^b r\, dr W(r) = 1. \tag{31}$$

The Fourier transform of Eq. (29) with respect to θ, z, t gives

$$\rho_{np}(r, \omega) = q\lambda_n \delta(\omega - \omega_0 n) H_p W(r), \tag{32}$$

with

$$J_{\theta np}(r, \omega) = \frac{\beta c r \rho_{np}(r, \omega)}{R}, \tag{33}$$

$$\lambda_n = \frac{1}{2\pi} \int_0^{2\pi} e^{-in\theta} \lambda(\theta)\, d\theta. \tag{34}$$

Recall that by Eq. (10) the functions ρ and J_θ are to be expanded in $\sin \alpha_p(z+g)$, so that

$$H_p = \frac{1}{g} \int_{-g}^{g} dz H(z) \sin \alpha_p(z+g). \tag{35}$$

We assume for simplicity that the beam profile is symmetrical about the median plane, $H(z) = H(-z)$, in which case

$$H_p = \frac{1}{g} \sin \frac{\pi p}{2} \int_{-g}^{g} dz H(z) \cos \alpha_p z, \tag{36}$$

which is nonzero only for odd p. Consequently, only odd-p modes of the fields are excited, and we may forget the rest. To obtain explicit formulas for the integrals of Eqs. (21) and (22), we take a vertical ribbon beam,

$$W(r) = \frac{\delta(r-R)}{R}. \tag{37}$$

The generalization to allow an arbitrary $W(r)$ is not difficult, but in general requires numerical integration of Eqs. (21) and (22).

Using Eqs. (32), (33), and (37) in Eqs. (21) and (22), we find the particular solutions

$$e_{znp}(r) = -\frac{\pi}{2} \Phi \alpha_p c Z_0 p_n(\gamma_p r, \gamma_p R) \theta(r-R), \tag{38}$$

$$h_{znp}(r) = -\frac{\pi}{2} \Phi \gamma_p \beta c q_n(\gamma_p r, \gamma_p R) \theta(r-R), \tag{39}$$

and their derivatives

$$e'_{znp}(r) = -\frac{\pi}{2} \Phi \alpha_p \gamma_p Z_0 r_n(\gamma_p r, \gamma_p R) \theta(r-R), \tag{40}$$

$$h'_{znp}(r) = -\frac{\pi}{2} \Phi \gamma_p^2 \beta c s_n(\gamma_p r, \gamma_p R) \theta(r-R) - \Phi \beta c \frac{\delta(r-R)}{R}, \tag{41}$$

where

$$\Phi = qH_p\lambda_n\delta(\omega - n\omega_0),$$

$$\theta(x) = \begin{cases} 1, & x \geq 0 \\ 0, & x < 0 \end{cases},$$

and, in the notation of Abramowitz and Stegun,[21] the Bessel function cross products are

$$p_n(x, y) = J_n(x)Y_n(y) - Y_n(x)J_n(y), \tag{42}$$

$$q_n(x, y) = J_n(x)Y_n'(y) - Y_n(x)J_n'(y), \tag{43}$$

$$r_n(x, y) = J_n'(x)Y_n(y) - Y_n'(x)J_n(y), \tag{44}$$

$$s_n(x, y) = J_n'(x)Y_n'(y) - Y_n'(x)J_n'(y). \tag{45}$$

The longitudinal coupling impedance, $Z(n, \omega)$, is defined by

$$-2\pi R\langle E_{\theta n}(\omega)\rangle = Z(n, \omega)I_{\theta n}(\omega), \tag{46}$$

where the angle brackets denote an average over the beam cross section. If we suppose that the beam is confined to a rectangle of area $\delta\omega \times \delta h$, we have

$$\langle E_{\theta n}(\omega)\rangle = \frac{1}{\delta w\, \delta h}\int_{R-\delta w/2}^{R+\delta w/2} dr \int_{-\delta h/2}^{\delta h/2} dz E_{\theta n}(r, z, \omega). \tag{47}$$

Some authors take the value of the field at the center of the beam rather than this average; the difference is usually not important. The Fourier amplitude of the current, $I_{\theta n}(\omega)$ is given in the model of Eq. (33) as

$$I_{\theta n}(\omega) = \int_a^b dr \int_{-g}^{g} dz J_{\theta n}(r, z, \omega) = \frac{\beta cq\lambda_n\, \delta(\omega - n\omega_0)}{R}. \tag{48}$$

We can now assemble the longitudinal electric field from Eqs. (14), (26), (27), (38), and (41). The result is

$$\begin{aligned} E_{\theta n}(r, \omega) = i\frac{\pi}{2} q\beta c\lambda_n\, \delta(\omega - n\omega_0)Z_0 \sum_{p=1}^{\infty} H_p \sin \alpha_p(z + g) \\ \times \left\{ \frac{\omega}{c}\left[-\frac{J_n'(\gamma_p r)}{J_n'(\gamma_p b)} s_n(\gamma_p b, \gamma_p R) + s_n(\gamma_p r, \gamma_p R)\theta(r - R) \right] \right. \\ \left. + \frac{1}{\beta}\left(\frac{\alpha_p}{\gamma_p}\right)^2 \frac{n}{r}\left[-\frac{J_n(\gamma_p r)}{J_n(\gamma_p b)} p_n(\gamma_p b, \gamma_p R) + p_n(\gamma_p r, \gamma_p R)\theta(r - R) \right] \right\}. \end{aligned} \tag{49}$$

Notice that the term $J_{\theta np}$ has been cancelled by the second term of h_{znp}'. The terms in Eq. (49) with factor $\theta(r - R)$ tend to zero as r tends to R from above. Therefore E_θ is continuous in r at $r = R$ but has a discontinuous derivative. The derivative would be continuous if Eq. (37) were replaced by an r-distribution of finite width.

From Eqs. (40)–(49), we calculate the impedance, divided by n:

$$\frac{Z(n,\omega)}{n} = 2i\pi^2 Z_0 \frac{R}{h} \sum_{p(\text{odd})\geq 1} \Lambda_p \times \left[\frac{\omega R}{cn} \frac{J_n'(\gamma_p R)}{J_n'(\gamma_p b)} s_n(\gamma_p b, \gamma_p R) + \frac{1}{\beta} \left(\frac{\alpha_p}{\gamma_p} \right)^2 \frac{J_n(\gamma_p R)}{J_n(\gamma_p B)} p_n(\gamma_p b, \gamma_p R) \right], \tag{50}$$

where

$$\Lambda_p = (-1)^{(p-1)/2} \frac{h}{2} \frac{\sin[(\pi p\ \delta h)/2h]}{(\pi p\ \delta h)/2h} H_p. \tag{51}$$

If $H(z)$ is rectangular (i.e., constant over a width δh and zero elsewhere) then

$$\Lambda_p = \left(\frac{\sin[(\pi p\ \delta h)/2h]}{(\pi p\ \delta h)/2h} \right)^2. \tag{52}$$

We use this model of $H(z)$ for specific evaluations of the impedance. Smoother functions will lead to faster convergence of the sum over p, but that feature is not very significant. The most important contributions, far and away, are from resonances in modes with $p = 1$.

3. FIELDS AND LONGITUDINAL COUPLING IMPEDANCE FOR A TOROIDAL CHAMBER

We now modify the work of the previous section to treat fields in the toroidal chamber shown in Fig. 1 with $a \neq 0$. The only new feature concerns the boundary conditions on the inner cylindrical wall, $r = a$. As in Eqs. (24) and (25), these conditions are satisfied if

$$E_{znp}(a) = 0, \quad \frac{\partial H_{znp}(a)}{\partial r} = 0. \tag{53}$$

The four conditions of Eqs. (25) and (53) serve to determine the four coefficients A_{np}, B_{np}, C_{np}, D_{np} in the general solutions [Eqs. (19) and (20)] of the radial wave equations. The function $Y_n(\gamma_p r)$ is now allowed, because its singularity at $r = 0$ is outside the chamber.

Through Eqs. (21) and (22) we have constructed the particular solutions so that $e_{znp}(a) = 0$, $h'_{znp}(a) = 0$. This simplifies solution of the equations for the coefficients, and we find

$$\begin{bmatrix} A_{np} \\ B_{np} \end{bmatrix} = \frac{e_{znp}(b)}{p_n(\gamma_p a, \gamma_p b)} \begin{bmatrix} Y_n(\gamma_p a) \\ -J_n(\gamma_p a) \end{bmatrix}, \tag{54}$$

$$\begin{bmatrix} C_{np} \\ D_{np} \end{bmatrix} = \frac{h'_{znp}(b)}{\gamma_p s_n(\gamma_p a, \gamma_p b)} \begin{bmatrix} Y_n'(\gamma_p a) \\ -J_n'(\gamma_p a) \end{bmatrix}, \tag{55}$$

where the Bessel function cross products, p_n and s_n, are as defined in Eqs. (42) and (45). Hence the solution for general sources, analogous to Eqs. (26) and (27),

is

$$E_{znp}(r) = \frac{p_n(\gamma_p r, \gamma_p a)}{p_n(\gamma_p a, \gamma_p b)} e_{znp}(b) + e_{znp}(r), \tag{56}$$

$$H_{znp}(r) = \frac{q_n(\gamma_p r, \gamma_p a)}{\gamma_p s_n(\gamma_p a, \gamma_p b)} h'_{znp}(b) + h_{znp}(r). \tag{57}$$

These fields tend properly to the values of Eqs. (26) and (27) in the limit $a \to 0$, as is seen by applying the asymptotes

$$J_n(x) \sim \frac{(x/2)^n}{\Gamma(n+1)}, \quad Y_n(x) \sim -\frac{1}{\pi}\frac{\Gamma(n)}{(x/2)^n}, \qquad x \to 0, \quad n > 0. \tag{58}$$

and corresponding asymptotes of $J'_n(x)$, $Y'_n(x)$.

Now comparing Eqs. (56) and (57) with Eqs. (26) and (27), we see that to write the longitudinal field $E_{\theta n}$ we only have to replace factors in Eq. (49) as follows:

$$\frac{-J'_n(\gamma_p r)}{J'_n(\gamma_p b)} \to \frac{s_n(\gamma_p r, \gamma_p a)}{s_n(\gamma_p a, \gamma_p b)}, \tag{59}$$

$$\frac{-J_n(\gamma_p r)}{J_n(\gamma_p b)} \to \frac{p_n(\gamma_p r, \gamma_p a)}{p_n(\gamma_p a, \gamma_p b)}. \tag{60}$$

Thus, for the vertical ribbon beam with r-distribution as in Eq. (37), the longitudinal coupling impedance of the toroidal chamber is given by

$$\frac{Z(n, \omega)}{n} = -2i\pi^2 Z_0 \frac{R}{h} \sum_{p(\text{odd}) \geq 1} \Lambda_p \times \left[\frac{\omega R}{cn} \frac{s_n(\gamma_p R, \gamma_p a) s_n(\gamma_p b, \gamma_p R)}{s_n(\gamma_p a, \gamma_p b)} + \frac{1}{\beta} \left(\frac{\alpha_p}{\gamma_p} \right)^2 \frac{p_n(\gamma_p R, \gamma_p a) p_n(\gamma_p b, \gamma_p R)}{p_n(\gamma_p a, \gamma_p b)} \right]. \tag{61}$$

Not only does Eq. (61) reduce to Eq. (50) in the limit $a \to 0$, but also it has similar characteristics even when $(b-a)/b \ll 1$, as we shall see in the following section.

4. EVALUATION OF IMPEDANCE AT LOW FREQUENCY

We are interested in the coupling impedance $Z(n, \omega)$ primarily for $\omega = n\omega_0$, since beam stability is affected mostly by waves with phase velocity close to the particle velocity. Therefore we first study $Z(n, n\omega_0)$ as a function of n. Later we shall look at $Z(n, \omega)$ in the (n, ω) plane, in a band about the line $\omega = n\omega_0$. That will clarify the properties of the function and will perhaps be important in a careful study of stability based on the Vlasov equation.

Let us first evaluate $Z(n, n\omega_0)/n$ at low frequency, which is to say in the limit $n \to 0$. In this limit, Γ_p^2 of Eq. (18) is positive for all p, which means that it is best

to rewrite the impedance in terms of modified Bessel functions before proceeding. Since

$$I_n(iz) = i^n J_n(z),$$
$$K_n(iz) = \frac{\pi}{2}(-i)^{n+1}[J_n(z) - iY_n(z)], \tag{62}$$

we have, in view of $\gamma_p^2 = -\Gamma_p^2$, that

$$I_n(\Gamma_p a)K_n(\Gamma_p b) - K_n(\Gamma_p a)I_n(\Gamma_p b) = -\frac{\pi}{2}p_n(\gamma_p a, \gamma_p b) = P_n(\Gamma_p a, \Gamma_p b),$$
$$I_n'(\Gamma_p a)K_n'(\Gamma_p b) - K_n'(\Gamma_p a)I_n'(\Gamma_p b) = \frac{\pi}{2}s_n(\gamma_p a, \gamma_p b) = S_n(\Gamma_p a, \Gamma_p b). \tag{63}$$

Extending the notation of Eqs. (42)–(45), we use capital letters for cross products of modified Bessel functions. The pillbox impedance of Eq. (50) becomes

$$\frac{Z(n, n\omega_0)}{n} = 4i\pi Z_0 \frac{R}{h} \sum_{p(\text{odd})\geq 1} \Lambda_p \left[\beta \frac{I_n'(\Gamma_p R)}{I_n'(\Gamma_p b)} S_n(\Gamma_p b, \Gamma_p R) + \frac{1}{\beta}\left(\frac{\alpha_p}{\Gamma_p}\right)^2 \frac{I_n(\Gamma_p R)}{I_n(\Gamma_p b)} P_n(\Gamma_p b, \Gamma_p R)\right], \tag{64}$$

whereas the torus impedance of Eq. (61) is

$$\frac{Z(n, n\omega_0)}{n} = -4i\pi Z_0 \frac{R}{h} \sum_{p(\text{odd})\geq 1} \Lambda_p \left[\beta \frac{S_n(\Gamma_p R, \Gamma_p a)S_n(\Gamma_p b, \Gamma_p R)}{S_n(\Gamma_n a, \Gamma_p b)} + \frac{1}{\beta}\left(\frac{\alpha_p}{\Gamma_p}\right)^2 \frac{P_n(\Gamma_p R, \Gamma_p a)P_n(\Gamma_p b, \Gamma_p R)}{P_n(\Gamma_p a, \Gamma_p b)}\right], \tag{65}$$

where

$$\Gamma_p^2 = \left(\frac{\pi p}{h}\right)^2 - \left(\frac{\beta n}{R}\right)^2. \tag{66}$$

To evaluate these expressions at $n = 0$, we need only the elementary asymptotic expansions of I_n and K_n for large argument. We assume, of course, that R, a, and b are all of the same order of magnitude and much bigger than w and h, as in a typical accelerator vacuum chamber; w is similar to h in magnitude. Then $\Gamma_p R = \pi p R/h$ is large compared to one, even at $p = 1$, which means that all of the Bessel functions can be evaluated by means of the asymptotic series (A.–S., 9.7.1–9.74),

$$I_n(x) \sim (2\pi x)^{-1/2} e^x \left[1 - \frac{4n^2 - 1}{8x} + \cdots\right], \tag{67}$$

$$K_n(x) \sim (2x/\pi)^{-1/2} e^{-x} \left[1 + \frac{4n^2 - 1}{8x} + \cdots\right], \tag{68}$$

$$I_n'(x) \sim (2\pi x)^{-1/2} e^x \left[1 - \frac{4n^2 + 3}{8x} + \cdots\right], \tag{69}$$

$$K_n'(x) \sim -(2x/\pi)^{-1/2} e^{-x} \left[1 + \frac{4n^2 + 3}{8x} + \cdots\right]. \tag{70}$$

The two terms in the square bracket of Eq. (64) are as follows at $n = 0$, $\Gamma_p = \alpha_p$:

$$\beta I_0'(\alpha_p R)K_0'(\alpha_p R)\left[1 - \frac{K_0'(\alpha_p b)I_0'(\alpha_p R)}{I_0'(\alpha_p b)K_0'(\alpha_p R)}\right]$$
$$= -\frac{\beta}{2\alpha_p R}\left[1 - \frac{3}{8(\alpha_p R)^2} + O\left(\frac{1}{(\alpha_p R)^4}\right)\right]\left\{1 - e^{-2\alpha_p(b-R)}\left[1 + O\left(\frac{1}{(\alpha_p R)^2}\right)\right]\right\}, \quad (71)$$

$$\frac{1}{\beta} I_0(\alpha_p R)K_0(\alpha_p R)\left[1 - \frac{K_0(\alpha_p b)I_0(\alpha_p R)}{I_0(\alpha_p b)K_0(\alpha_p R)}\right]$$
$$= \frac{1}{\beta}\frac{1}{2\alpha_p R}\left[1 + \frac{1}{8(\alpha_p R)^2} + O\left(\frac{1}{(\alpha_p R)^4}\right)\right]\left\{1 - e^{-2\alpha_p(b-R)}\left[1 + O\left(\frac{1}{(\alpha_p R)^2}\right)\right]\right\} \quad (72)$$

The terms indicated by the O symbol are negligible, since $1/(\alpha_p R)^2 = (h/\pi p R)^2 \ll 1$. Also, the terms with the exponential factor $\exp[-2\alpha p(b - R)]$ are usually small, certainly if $2(b - R)/h \geq 1$, as is the case in our later examples. Dropping the exponential terms, we find

$$\left.\frac{Z(n, n\omega_0)}{n}\right|_{n=0} = \frac{2iZ_0}{\beta} \sum_{p(\text{odd})\geq 1} \frac{\Lambda_p}{p} \cdot \left[\frac{1}{\gamma^2} + \frac{3\beta^2 + 1}{8}\left(\frac{h}{\pi p R}\right)^2\right]. \quad (73)$$

The corresponding result for the torus impedance [Eq. (65)] is exactly the same as Eq. (73). The exponential terms that we have deleted are different in the two cases; for high accuracy they should be reinstated, at least for $p = 1$.

The first term in Eq. (73), which vanishes in the relativistic limit as $1/\gamma^2$, corresponds to the familiar coupling impedance of a smooth straight tube without wall resistance. It is sometimes called the "space-charge" contribution to the impedance. Notice that the $1/\gamma^2$ was produced by a close cancellation between the two terms in E_θ, one of which arises from H_{znp}, the other from E_{znp}. The second term in Eq. (73) is due to curvature of the particle trajectory, which spoils the perfect cancellation of electric and magnetic effects at large γ.

The total low-frequency impedance [Eq. (73)] is positive imaginary (capacitive in a common convention) and, except for nonrelativistic particles, quite small by usual standards. For instance, for $\delta h/h = 0{\cdot}05$, the sums occurring in Eq. (43) have the approximate values

$$\sum_{p(\text{odd})\geq 1} \frac{\Lambda_p}{p} = 2{\cdot}022; \qquad \frac{1}{2\pi^2} \sum_{p(\text{odd})\geq 1} \frac{1}{p^3} \Lambda_p = 0{\cdot}05305, \quad (74)$$

where Λ_p is given by Eq. (52).

Then, in this example with $\beta \approx 1$, we have

$$\left.\frac{Z(n, n\omega_0)}{n}\right|_{n=0} = iZ_0\left[\frac{4.044}{\gamma^2} + 0.1061\left(\frac{h}{R}\right)^2\right], \quad (75)$$

which is typically a very small fraction of an ohm.

An analysis of the intermediate region up to the resonances, in which the order of magnitude of the impedance is much the same as at zero frequency, requires more powerful asymptotic expansions than Eqs. (67)–(70). The somewhat complicated analysis is given in Ref. 25. Here we shall be content with the claim that direct numerical evaluation of the Olver asymptotic expansions (Section 5) leads to values of the impedance that are negligible until the high-frequency resonant values are reached. Of course, in this statement we suppose that γ^2 is large compared to one, so that the space-charge term is negligible. Also, we neglect the resistive-wall effect, which can be treated easily only at frequencies near resonances. Presumably, it has the same order of magnitude as in the case of a straight beam tube.

5. RESONANCE POLES OF THE IMPEDANCE AT HIGH FREQUENCY

Let us now turn to the more interesting topic of high-frequency resonances, first in connection with Eq. (50) for the pillbox chamber. The resonances correspond to zeros of the denominators, $J_n'(\gamma_p b)$ and $J_n(\gamma_p b)$, and poles of the impedance. As can be seen from the discussion of Section 2, the resonances correspond to solutions of the *homogeneous* Maxwell equations that satisfy the boundary conditions. There are two classes of such solutions:

$$\text{(i) TE modes:} \quad E_z \equiv 0, \quad H_z \neq 0, \quad J_n'(\gamma_p b) = 0, \tag{76}$$

$$\text{(ii) TM modes:} \quad H_z \equiv 0, \quad E_z \neq 0, \quad J_n(\gamma_p b) = 0. \tag{77}$$

The designation TE (TM) refers to a mode with electric (magnetic) field *transverse* to the z-axis, not transverse to the beam, which moves in the θ direction. This nomenclature is natural in our peculiar coordinate system but contrary to the convention of wave-guide theory if the torus is viewed as a wave guide. As is seen from Eqs. (11)–(14), in a pure TE (TM) mode, all fields *except* $E_z(H_z)$ are nonzero.

Although the TE and TM modes are independent solutions of the homogeneous Maxwell equations, our circulating beam is simultaneously a source for both E_z and H_z (through ρ and J_θ, respectively), so that the fields driven by the beam always have both TE and TM components. Nevertheless, at a resonance frequency, one component or the other dominates, in fact becomes infinite, for a chamber of perfect conductivity.

As we shall see presently, near a resonance frequency ω_r the impedance for the perfectly conducting chamber has the form

$$Z(n, \omega) \sim \frac{i\zeta}{\omega - \omega_r}, \qquad \omega \to \omega_r, \tag{78}$$

where the factor ζ is real and positive, and ω_r is real. When resistivity of the chamber walls is introduced, the pole moves off the real ω axis into the lower

half complex plane:

$$\omega_r \to \omega_r\left(1 - \frac{i}{2Q}\right). \tag{79}$$

The quantity Q may be identified with the usual quality factor. With resistivity, the factor ζ also picks up a small imaginary part but stays predominantly real. To a good approximation, Eq. (78) takes the form

$$Z(n, \omega) \sim \frac{i\,|\zeta|\left[\omega - \omega_r\left(1 + \frac{i}{2Q}\right)\right]}{(\omega - \omega_r)^2 + \left(\frac{\omega_r}{2Q}\right)^2}, \tag{80}$$

with real part of Lorentzian form

$$\mathscr{R} = \operatorname{Re} Z(n, \omega) \sim \frac{|\zeta|\frac{\Gamma}{2}}{(\omega - \omega_r)^2 + \left(\frac{\Gamma}{2}\right)^2}, \tag{81}$$

having a half-width at half-maximum of $\Gamma/2 = \omega_r/2Q$. The value of $\mathscr{R}/Q$ at the resonance is

$$\frac{\mathscr{R}}{Q} = \frac{\operatorname{Re} Z(n, \omega_r)}{Q} = \frac{2\,|\zeta|}{\omega_r} \approx \frac{2\zeta}{\omega_r}\bigg|_{\sigma=\infty}. \tag{82}$$

Thus $\mathscr{R}/Q$ may be computed from the two parameters ζ and ω_r that characterize the chamber with infinite conductivity. Also, the area under the curve of $\operatorname{Re} Z(n, \omega)$, in the limit $Q \to \infty$, is

$$\lim_{Q\to\infty} \int d\omega \operatorname{Re} Z(n, \omega) = \pi\zeta = \frac{\pi\omega_r}{2}\frac{\mathscr{R}}{Q}, \tag{83}$$

where the integral covers a small neighborhood of ω_r.

Our task for the rest of this section is to find the resonance frequencies ω_r and residues ζ (equivalently ω_r and $\mathscr{R}/Q$) for the perfectly conducting chamber. The values of Q are discussed in Section 6.

The above discussion of TE and TM resonances holds as well for the torus problem, except that the resonance conditions are replaced by

$$s_n(\gamma_p a, \gamma_p b) = 0, \qquad \text{(TE)}, \tag{84}$$

$$p_n(\gamma_p a, \gamma_p b) = 0, \qquad \text{(TM)}. \tag{85}$$

Again, these equations just guarantee the boundary conditions on solutions of the homogeneous Maxwell equations.

The impedance $Z(n, \omega)$ has a dense forest of poles in the (n, ω) plane, but we

are interested only in the subset of poles sufficiently close to points of the form $(n, n\omega_0)$ to have some effect on beam stability. Except for isolated values of ω_0, such points $(n, n\omega_0)$ do not fall exactly on poles. To locate relevant poles, we let ω_0 be arbitrary and treat n as a continuous variable, not restricted to integer values. This is permissible as a trick to find poles, since the impedance is analytic in n. Having found a pole for noninteger $n = n_r$, which will be very large compared to one, we can then look at $Z(n, n\omega_0)$ for neighboring integer values of n and as a function of ω_0.

The first zero of the Bessel function $J_n(x)$ [or of $J_n'(x)$] occurs at x slightly bigger than the order n. The reason for this is almost apparent in the Bessel equation itself:

$$\frac{1}{x}\frac{\partial}{\partial x}\left(x\frac{\partial f}{\partial x}\right)+\left(1-\frac{n^2}{x^2}\right)f=0. \tag{86}$$

By analogy to the harmonic oscillator, it seems reasonable that the solutions should have oscillatory character only if $1-n^2/x^2$ is positive. In a region with $1-n^2/x^2$ negative, there should be one increasing solution and one decreasing solution.

With this observation we can immediately set the scale of interesting values of n. At $\omega = \omega_0 n$,

$$\gamma_p b=\left[\left(\frac{\beta n}{R}\right)^2-\left(\frac{\pi p}{h}\right)^2\right]^{1/2} b. \tag{87}$$

Putting $\gamma_p b = n$ we find

$$n^2=\frac{\left(\frac{\pi p b}{h}\right)^2}{\left(\frac{\beta b}{R}\right)^2-1}. \tag{88}$$

Since b/R is close to one, this means first of all that β must be close to one, in order that n^2 be positive; compare Eq. (3). Nonrelativisic particles cannot excite the resonances of interest. If we then put $\beta = 1$, and suppose that $b = R + x/2$, with $x \ll R$, we can expand the denominator in Eq. (88) as

$$\left(\frac{\beta b}{R}\right)^2-1=\frac{x}{R}+\frac{x^2}{4R^2}\approx\frac{x}{R}, \tag{89}$$

Then by Eq. (88),

$$n>\frac{\pi p b}{h}\left(\frac{R}{x}\right)^{1/2}, \qquad b-R=\frac{x}{2}, \tag{90}$$

is a lower bound for resonant values of n for each p. The value goes up without bound as the beam approaches the outer wall, $x \to 0$. We shall find that this same lower bound applies to the torus resonances.

To illustrate, we take chamber dimensions that are nominal values for two electron storage rings, the SLAC damping ring and the forthcoming Lawrence Berkeley Laboratory Advanced Light Source (ALS). Henceforth, these examples

are called (1) and (2):

$$\begin{aligned} &(1)\quad w = h = 2\,\text{cm}, && R = 5.7\,\text{m} && \text{(SLAC)},\\ &(2)\quad w = 5\,\text{cm}, \quad h = 2.5\,\text{cm}, && R = 30\,\text{m} && \text{(ALS)}. \end{aligned} \tag{91}$$

If the beam is centered in the chamber, then $x = w$ in Eq. (90), and

$$\begin{aligned} &(1)\quad n > 15141 \times p,\\ &(2)\quad n > 92420 \times p. \end{aligned} \tag{92}$$

The values of n are so large that well-known asymptotic expansions of Bessel functions for large order give precise results when only the initial terms of the asymptotic series are used. We write

$$\gamma_p b = nz, \tag{93}$$

and use expansions of $J_n(nz)$ *et al.* that hold at large n. The biggest value of z that occurs is obtained from Eq. (87):

$$z_{\max} = \lim_{n\to\infty} \frac{\gamma_p b}{n} = \frac{\beta b}{R}. \tag{94}$$

In the resonance region, z in Eq. (93) is never less than one, but we have to deal also with $J_n(\gamma_p a)$, $J_n(\gamma_p R)$ *et al.*, $a < R < b$. To cover all cases in the resonance region we therefore need $J_n(nz)$, $Y_n(nz)$, $J_n'(nz)$, $Y_n'(nz)$, where z may be restricted to the interval

$$\frac{a}{b} < z < \frac{b}{R}. \tag{95}$$

The behavior of the high-order Bessel functions varies drastically within this seemingly narrow interval of z, a circumstance that leads us to employ expansions that are uniformly accurate throughout the interval.

We use the remarkable asymptotic expansions of Olver, which are uniform in a much bigger domain, the whole complex z-plane minus a narrow wedge about the negative real axis; i.e., $|argz| \le \pi - \epsilon$, for any $\epsilon > 0$. The Olver expansions are given in A.–S. (9.3.35, 9.3.36, 9.3.43, 9.3.44) and, in a more sophisticated form with error bounds, in Refs. 22 and 23. The expansion of J_n, accurate uniformly in z at large n, is

$$J_n(nz) \sim \left(\frac{4\zeta}{1-z^2}\right)^{1/4}\left[\frac{\mathrm{Ai}(n^{2/3}\zeta)}{n^{1/3}}\sum_{k=0}^{\infty}\frac{a_k(\zeta)}{n^{2k}} + \frac{\mathrm{Ai}'(n^{2/3}\zeta)}{n^{5/3}}\sum_{k=0}^{\infty}\frac{b_k(\zeta)}{n^{2k}}\right], \tag{96}$$

where $\mathrm{Ai}(x)$ is the Airy function [Ref. 21, (10.4)], and ζ is defined by

$$\begin{aligned} \frac{2}{3}\zeta^{3/2} &= \ln\frac{1+(1-z^2)^{1/2}}{z} - (1-z^2)^{1/2}\\ &= (1-z^2)^{3/2}\left[\frac{1}{3} + \frac{1}{5}(1-z^2) + \frac{1}{7}(1-z^2)^2 + \cdots\right]. \end{aligned} \tag{97}$$

We have $a_0(\zeta) = 1$, and the higher coefficients a_k and b_k are given in Ref. 21, but in a form difficult to evaluate numerically owing to cancellations among terms that are singular at $z = 1$. Actually, these coefficients are analytic near $z = 1$ and can be computed easily from their Taylor series about $z = 1$. Conveniently, Decker[19] has provided numerical values for the coefficients of the Taylor series.

The Airy functions Ai, Ai′ in Eq. (96) can be expressed in terms of Bessel functions of small fractional orders ($\pm 1/3$, $\pm 2/3$, respectively). Consequently, they can be evaluated by using asymptotic series at large arguments and power series at small arguments. Since $n^{2/3}\zeta$ is large and positive for z in the lower end of the interval [Eq. (95)], large and negative in the upper end, and zero in between at $z = 1$, we must use three means of calculating the Airy functions; namely Ref. 21 (10.4.59) and (10.4.60) for large positive and negative arguments, respectively, and the power series Ref. 21 (10.4.2) near $z = 1$.

We have written a computer program that makes these evaluations of Airy functions and uses Decker's form of the coefficients to evaluate the Olver formulas for J_n, Y_n, J_n', and Y_n'. It allows z to be complex, since complex z arises later in the study of wall resistance. To validate the program, we have checked the Airy functions against published tables and have verified that the Bessel functions satisfy recursion relations and the Wronskian identity. Also, the Bessel functions agree with simpler, but less comprehensive, asymptotic formulas at large n. In Figs 2–5 we show the Bessel functions near $z = 1$ for $n = 23051$, the value of n corresponding to the lowest resonance with $\omega = \omega_0 n$ in example (1) of Eq. (91).

Although the program was used for all numerical work, it is possible to see how the resonant frequencies are determined by looking just at the leading terms. In fact, most of the program was hardly necessary for our main results, since leading terms dominate strongly. For Bessel functions of $\gamma_p b$ we have $z > 1$ and $n^{2/3}\zeta$ large and negative. The leading terms for this case are, with $\gamma_p b = nz$,

$$\begin{aligned}
J_n(nz) &\sim \left(\frac{2}{\pi n}\right)^{1/2} (z^2-1)^{-1/4} \sin\left(n\chi + \frac{\pi}{4}\right) + O(n^{-3/2}),\\
Y_n(nz) &\sim -\left(\frac{2}{\pi n}\right)^{1/2} (z^2-1)^{-1/4} \cos\left(n\chi + \frac{\pi}{4}\right) + O(n^{-3/2}),\\
J_n'(nz) &\sim \left(\frac{2}{\pi n}\right)^{1/2} \frac{(z^2-1)^{1/4}}{z} \cos\left(n\chi + \frac{\pi}{4}\right) + O(n^{-3/2}),\\
Y_n'(nz) &\sim \left(\frac{2}{\pi n}\right)^{1/2} \frac{(z^2-1)^{1/4}}{z} \sin\left(n\chi + \frac{\pi}{4}\right) + O(n^{-3/2}),
\end{aligned} \tag{98}$$

where

$$\chi = \frac{2}{3}(-\zeta)^{3/2} = (z^2-1)^{3/2}\left[\frac{1}{3} + \frac{1}{5}(1-z^2) + \frac{1}{7}(1-z^2)^2 + \cdots\right]. \tag{99}$$

For Bessel functions of $\gamma_p a$ we have $z < 1$ and $n^{2/3}\zeta$ large and positive. The

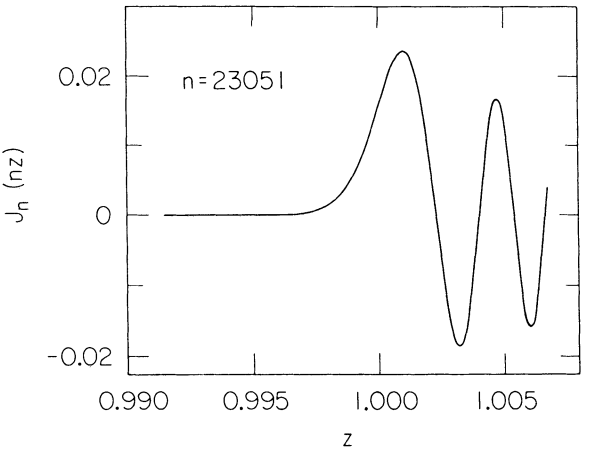

FIGURE 2

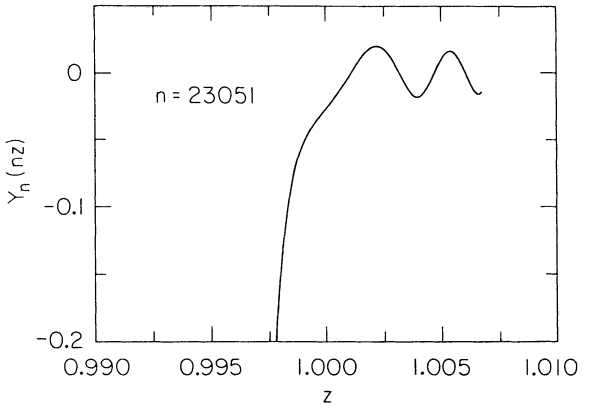

FIGURE 3

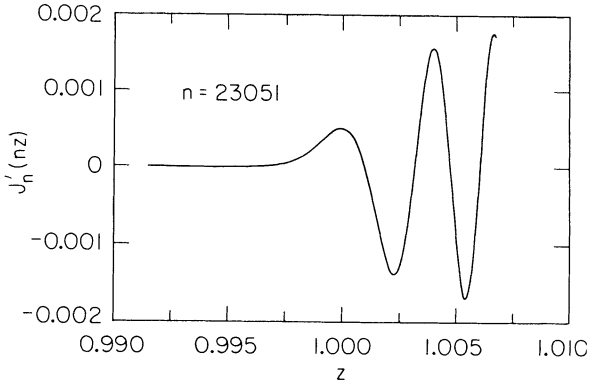

FIGURE 4

FIGURES 2–5 Bessel functions and their derivatives at large order, with argument close to the order. The order $n = 23051$ corresponds to the lowest TE mode [example (1) from Eq. (91)].

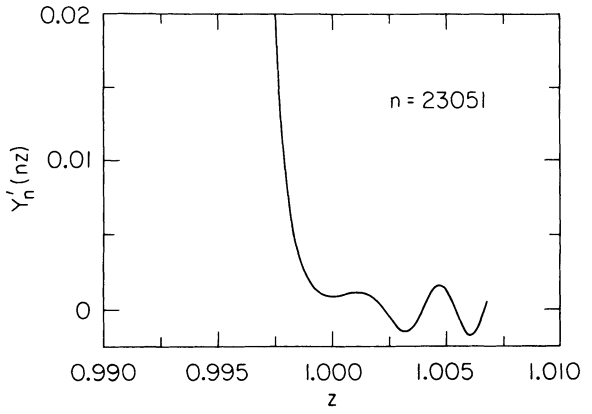

FIGURE 5

leading terms for this case are, with $\gamma_p a = nz$,

$$\begin{aligned} J_n(nz) &\sim \left(\frac{1}{2\pi n}\right)^{1/2}(1-z^2)^{-1/4}\,e^{-n\xi} + O(n^{-3/2}), \\ Y_n(nz) &\sim -\left(\frac{2}{\pi n}\right)^{1/2}(1-z^2)^{-1/4}e^{n\xi} + O(n^{-3/2}), \\ J_n'(nz) &\sim \left(\frac{1}{2\pi n}\right)^{1/2}\frac{(1-z^2)^{1/4}}{z}\,e^{-n\xi} + O(n^{-3/2}), \\ Y_n'(nz) &\sim \left(\frac{2}{\pi n}\right)^{1/2}\frac{(1-z^2)^{+1/4}}{z}\,e^{n\xi} + O(n^{-3/2}), \end{aligned} \tag{100}$$

where

$$\xi = \frac{2}{3}\zeta^{3/2} = (1-z^2)^{3/2}\left[\frac{1}{3} + \frac{1}{5}(1-z^2) + \frac{1}{7}(1-z^2)^2 + - \right]. \tag{101}$$

Equations (100) are in agreement with the claim made above, that the Bessel functions do not have zeros for argument less than n. The oscillatory functions of Eq. (98) do have zeros, which we shall now try to locate.

By Eq. (98) and Eqs. (76) and (77), the resonances for the pillbox should be close to the values of n for which

$$\begin{aligned} n\chi &= \left(\frac{q}{4} + s\right)\pi, \qquad s = 0, 1, 2, \ldots, \\ q &= \begin{cases} 1 & \text{for TE modes,} \\ 3 & \text{for TM modes,} \end{cases} \end{aligned} \tag{102}$$

where $\chi = \chi(n, p)$ is given by Eq. (99) with

$$z^2 = \left(\frac{\gamma_p b}{n}\right)^2 = \left(\frac{\beta b}{R}\right)^2 - \frac{1}{n^2}\left(\frac{\pi p b}{h}\right)^2. \tag{103}$$

The condition $\omega = \omega_0 n = \beta c n/R$ has been imposed in Eq. (103).

We first find an approximate solution of Eq. (102) by analytic means. We then take that approximation as the starting point for a precise solution of the resonance conditions [Eqs. (76) and (77)] by Newton's method, using the full Bessel function program. The derivative required in Newton's method is adequately approximated by a simple divided difference. The resulting precise resonant frequencies agree with those obtained from the analytic approximation to about 3% in the examples [Eq. (91)].

To find the approximate solution of Eq. (102), we put $u = z^2 - 1$ and retain just the first term in the series [Eq. (99)] for χ:

$$\chi \approx \frac{1}{3} u^{3/2}. \tag{104}$$

By Eq. (94) the largest possible value of u is $(b/R)^2 - 1$, which is usually small compared to one; hence, the higher terms in χ have little effect. Solving Eq. (103) for n as a function of u, we find

$$n = \frac{\dfrac{\pi p b}{h}}{\left[\left(\dfrac{\beta b}{R}\right)^2 - 1 - u\right]^{1/2}}. \tag{105}$$

Putting Eqs. (104) and (105) into Eq. (102), we obtain a cubic equation,

$$v + \lambda v^3 = 1, \tag{106}$$

where

$$u = \left[\left(\frac{\beta b}{R}\right)^2 - 1\right] v, \qquad \lambda = \left\{ \frac{pb\left[\left(\dfrac{\beta b}{R}\right)^2 - 1\right]}{3h\left(\dfrac{q}{4} + s\right)} \right\}^2. \tag{107}$$

This equation clearly has one, and only one, positive solution that is less than one. The solution determines the resonant value of n by Eq. (105). Applying the Cardan formulas for roots of a cubic, we find

$$v = \left[\frac{\left(1 + \dfrac{4}{27\lambda}\right)^{1/2} + 1}{2\lambda} \right]^{1/3} - \left[\frac{\left(1 + \dfrac{4}{27\lambda}\right)^{1/2} - 1}{2\lambda} \right]^{1/3}. \tag{108}$$

To find the resonances of the torus, we first observe that they are very close to the resonances of the pillbox, hence very close to the frequencies determined by Eq. (106). Thus, we can use the latter as a starting point for a Newtonian solution of the torus resonance conditions [Eqs. (84) and (85)], just as in the pillbox problem. To see why the torus resonances are close to those of the pillbox, note that the torus resonance condition (TM modes) is

$$\frac{Y_n(\gamma_p a)}{J_n(\gamma_p a)} J_n(\gamma_p b) - Y_n(\gamma_p b) = 0. \tag{109}$$

By Eqs. (98) and (100), this is nearly equivalent to

$$\tfrac{1}{2}e^{2n\xi}\sin(n\chi+\pi/4)-\cos(n\chi+\pi/4)=0. \tag{110}$$

The factor $e^{2n\xi}\approx Y_n(\gamma_p a)/J_n(\gamma_p a)$ is large compared to one at the value of n corresponding to the pillbox resonance. In example (1) of Eq. (91), in the lowest pillbox TM mode, we have

$$z_b=\frac{\gamma_p b}{n}=1.001526,\qquad z_a=\frac{\gamma_p a}{n}=0.99802,\qquad n=42282$$

$$\xi\approx\frac{1}{3}(1-z_a^2)^{3/2},\qquad e^{2n\xi}\approx 1124. \tag{111}$$

Since $e^{2n\xi}$ is so large, the solution of Eq. (110) is very close to the pillbox resonance, where $\sin(n\chi+\pi/4)=0$, $\cos(n\chi+\pi/4)=\pm 1$. The Bessel functions evaluated at $\gamma_p a$ are in their region of exponential behavior, where $|Y_n(\gamma_p a)|\gg|J_n(\gamma_p a)|$. This is illustrated in Figs. 6 and 7, where we plot $J_n(nz)$ and $Y_n(nz)$ for $a/b<z<b/R$ for the first TM mode of the pillbox.

Having located the poles, we next must calculate the pole residues to find $\mathcal{R}/Q$. We find analytic formulas for the residues in terms of Bessel functions and then evaluate them numerically. Near each pole we write the impedance as $Z(n,\omega)=iN(\omega)/D(\omega)$, $D(\omega)\approx D'(\omega_r)(\omega-\omega_r)$ and then simplify $N(\omega_r)/D'(\omega_r)$ by using the identities of Eqs. (23), (76), (77), (84), and (85). From Eq. (82) we obtain the following:

(A) Cylindrical Pillbox

$$\left.\frac{\mathcal{R}}{Q}\right|_{\mathrm{TE}}=2\pi^3 Z_0\Lambda_p\frac{c(\gamma_p R)^2}{\omega h}\frac{[Y_n'(\gamma_p b)J_n'(\gamma_p R)]^2}{1-z_b^{-2}}, \tag{112}$$

$$\left.\frac{\mathcal{R}}{Q}\right|_{\mathrm{TM}}=2\pi^5 Z_0\Lambda_p\frac{cp^2}{\omega h}\left(\frac{R}{\beta h}\right)^2[Y_n(\gamma_p b)J_n(\gamma_p R)]^2, \tag{113}$$

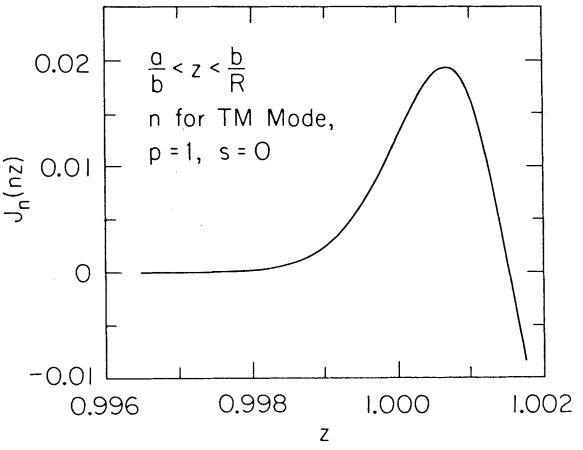

FIGURE 6

FIGURES 6–7 $J_n(nz)$ and $Y_n(nz)$ over the full range of z relevant for resonances: $a/b<z<b/R$ [example (1)].

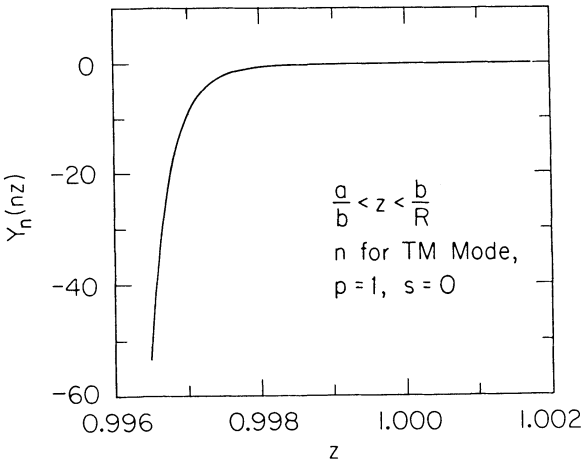

FIGURE 7

(B) Torus

$$\left.\frac{\mathscr{R}}{Q}\right|_{\mathrm{TE}} = 2\pi^3 Z_0 \Lambda_p \frac{c(\gamma_p R)^2}{\omega h} \frac{[J_n'(\gamma_p b)Y_n'(\gamma_p R) - Y_n'(\gamma_p b)J_n'(\gamma_p R)]^2}{1 - z_b^{-2} - (1 - z_a^{-2})\left[\dfrac{Y_n'(\gamma_p b)}{Y_n'(\gamma_p a)}\right]^2}, \tag{114}$$

$$\left.\frac{\mathscr{R}}{Q}\right|_{\mathrm{TM}} = 2\pi^5 Z_0 \Lambda_p \frac{cp^2}{\omega h}\left(\frac{R}{\beta h}\right)^2 \frac{[J_n(\gamma_p b)Y_n(\gamma_p R) - Y_n(\gamma_p b)J_n(\gamma_p R)]^2}{1 - \left[\dfrac{Y_n(\gamma_p b)}{Y_n(\gamma_p a)}\right]^2}, \tag{115}$$

where $\omega = \omega_r$, Λ_p is defined in Eq. (51), and

$$z_a = \frac{\gamma_p a}{n} < 1, \qquad z_b = \frac{\gamma_p b}{n} > 1. \tag{116}$$

In Table I, we show results for the first few resonances in the two examples of Eq. (91), with Λ_p as in Eq. (52). The beam is centered in the toroidal chamber: $R = (a + b)/2$. We give the integer closest to the resonant value of n, the corresponding frequency f in GHz ($f = \omega_0 n/2\pi$), and the value of $u = z^2 - 1$, where z^2 is defined in Eq. (103). The frequencies for the torus and pillbox are the same to better than 6 significant figures; consequently, the integer values of n are the same. Table I also gives $\mathscr{R}/Q$ for the torus and pillbox. The near agreement of the $\mathscr{R}/Q$ values for torus and pillbox is not surprising, in view of Eqs. (112)–(115) and the near equality of frequencies. For instance, the equality of frequencies means that the term involving $J_n'(\gamma_p b)$ in the numerator of Eq. (114) is small. Also, the term in the denominator involving Y_n' is small (see Fig. 7). Thus, (114) and (112) are approximately equal.

The physical similarily of the torus and pillbox problems is apparent in plots of the radial wave functions corresponding to solutions of the homogeneous Maxwell equations at resonance. At resonance, the latter are close to solutions of the inhomogeneous equations; the initial terms in Eqs. (26), (27), (56), and (57)

TABLE I

$p\,s$	n	f(GHz)	$u = z^2 = 1$	$R/Q(\Omega)$ Torus	$R/Q(\Omega)$ Pillbox	Q
Example (1): SLAC damping ring						
TE 1 0	23025	193	$1.99 \cdot 10^{-3}$	14.167	14.515	$5.91 \cdot 10^{4}$
TE 1 1	61841	518	$3.33 \cdot 10^{-3}$	4.8540	4.8554	$1.62 \cdot 10^{5}$
TE 1 2	105157	881	$3.44 \cdot 10^{-3}$	2.4296	2.4296	$2.18 \cdot 10^{5}$
TE 3 0	55002	461	$1.12 \cdot 10^{-3}$	0.29234	0.29366	$5.12 \cdot 10^{4}$
TE 3 1	88788	744	$2.59 \cdot 10^{-3}$	1.0319	1.0320	$1.51 \cdot 10^{5}$
TM 1 0	42286	354	$3.06 \cdot 10^{-3}$	3.1982	3.1990	$7.04 \cdot 10^{4}$
TM 1 1	83665	701	$3.34 \cdot 10^{-3}$	0.70394	0.70276	$9.90 \cdot 10^{4}$
TM 1 2	127595	1069	$3.46 \cdot 10^{-3}$	0.24870	0.24828	$1.22 \cdot 10^{5}$
TM 3 0	72536	607	$2.14 \cdot 10^{-3}$	0.57762	0.57700	$9.21 \cdot 10^{4}$
TM 3 1	107102	897	$2.88 \cdot 10^{-3}$	0.81308	0.81192	$1.12 \cdot 10^{5}$
Example (2): LBL advanced light source						
TE 1 0	119317	190	$6.67 \cdot 10^{-4}$	2.9212	2.9236	$1.03 \cdot 10^{5}$
TE 1 1	226279	360	$1.39 \cdot 10^{-3}$	3.7536	3.7536	$2.96 \cdot 10^{5}$
TE 1 2	347361	553	$1.55 \cdot 10^{-3}$	2.6816	2.6816	$4.09 \cdot 10^{5}$
TE 3 0	312047	497	$3.52 \cdot 10^{-4}$	$6.1348 \cdot 10^{-4}$	$9.9134 \cdot 10^{-4}$	$8.79 \cdot 10^{4}$
TE 3 1	415723	662	$9.26 \cdot 10^{-4}$	$2.4424 \cdot 10^{-2}$	$2.4492 \cdot 10^{-2}$	$2.67 \cdot 10^{5}$
TM 1 0	173425	276	$1.19 \cdot 10^{-3}$	2.6824	2.6810	$7.76 \cdot 10^{4}$
TM 1 1	286529	456	$1.49 \cdot 10^{-3}$	1.6449	1.6437	$9.98 \cdot 10^{4}$
TM 1 2	412078	656	$1.58 \cdot 10^{-3}$	0.84784	0.84718	$1.20 \cdot 10^{5}$
TM 3 0	368261	586	$7.23 \cdot 10^{-4}$	$6{\cdot}8362 \cdot 10^{-3}$	$6.8278 \cdot 10^{-3}$	$1.13 \cdot 10^{5}$
TM 3 1	466669	743	$1.08 \cdot 10^{-3}$	$5.0546 \cdot 10^{-2}$	$5.0510 \cdot 10^{-2}$	$1.27 \cdot 10^{5}$

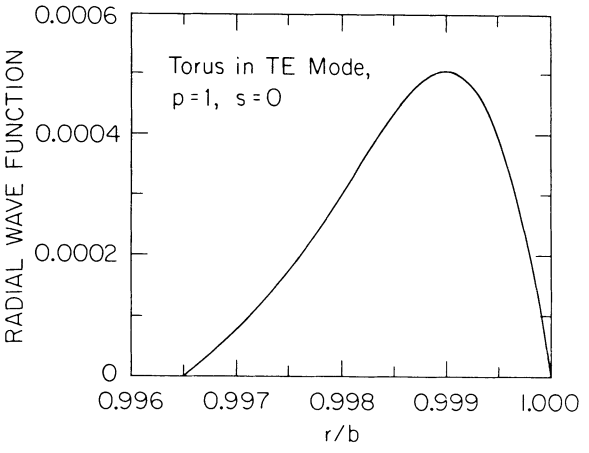

FIGURE 8 Radial wave function $s_n(\gamma_p r, \gamma_p a)$ in the lowest TE mode of the torus [example (1)].

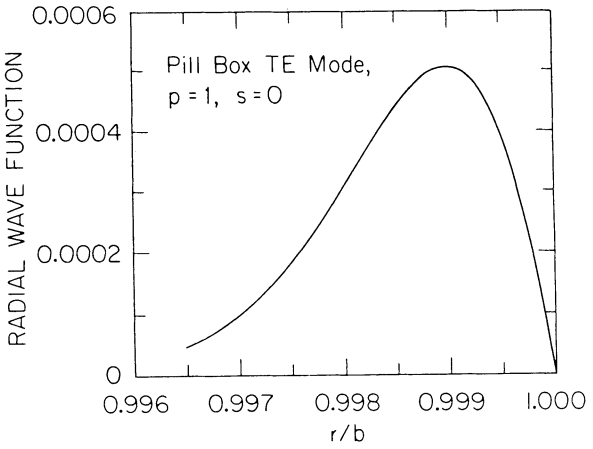

FIGURE 9 Radial wave function $J_n'(\gamma_p r)$ in the lowest TE mode of the pillbox [example (1)].

dominate. In Fig. 8 we plot the torus wave function $s_n(\gamma_p r,\ \gamma_p a) = J_n'(\gamma_p r)Y_n'(\gamma_p a) - Y_n'(\gamma_p r)J_n'(\gamma_p a)$ versus r at the lowest TE resonance; it vanishes at $r = a,\ b$, as required. Figure 9 shows the pillbox wave function $J_n'(\gamma_p r)$ at the same frequency. It is remarkably similar to the torus wave function. The similarity is even greater in higher radial modes. In Fig. 10 we show the torus wave function for the $p = 1,\ s = 2$ TE mode, which is indistinguishable by eye from the corresponding pillbox wave function. The pillbox wave function almost automatically satisfies the boundary condition $J_n'(\gamma_p a) = 0$ because of the exponential decrease of $J_n'(nz)$ with decreasing $z < 1$.

The similarity of the torus and pillbox resonant modes naturally disappears if the trajectory radius R is very close to the inner torus radius a.

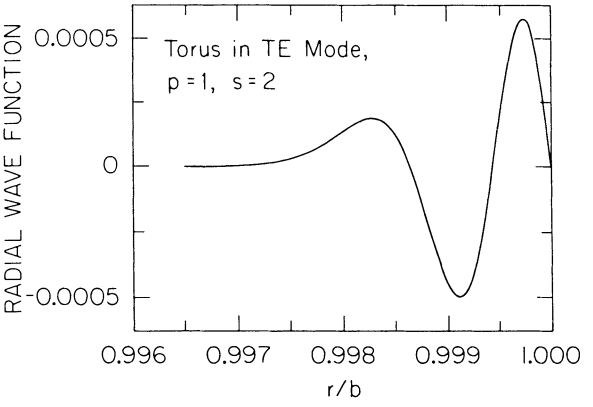

FIGURE 10 Radial wave function for torus or pillbox, in TE mode with $p = 1,\ s = 2$ [example (1)].

6. RESISTIVE-WALL BOUNDARY CONDITIONS AND COMPUTATION OF Q

To account for electrical resistance of the vacuum-chamber walls, we adopt the conventional resistive-wall boundary condition:

$$\mathbf{E}_{\|}(\omega) = \left[\frac{-i\omega\mu}{\sigma - i\omega\epsilon}\right]^{1/2} \mathbf{n} \times \mathbf{H}_{\|}(\omega), \tag{117}$$

where quantities written in boldface type are vectors. The fields $\mathbf{E}_{\|}$ and $\mathbf{H}_{\|}$ are the components of $\mathbf{E}$ and $\mathbf{H}$ parallel to the wall, and $\mathbf{n}$ is the unit vector normal to the wall, pointing away from the wall (into the vacuum). Within the wall material $\mathbf{J} = \sigma\mathbf{E}$, $\mathbf{D} = \epsilon\mathbf{E}$, $\mathbf{B} = \mu\mathbf{H}$. For the derivation of Eq. (117) it is assumed that the surface of the wall is planar and that the fields within the wall have negligible variation in directions parallel to the surface. The assumption of planarity is justified in our case because of the large radius of curvature of our cylindrical walls. The second assumption is not well justified near the corners, where planar and cylindrical walls of the vacuum chamber meet. We are forced to ignore that difficulty, since a correct treatment of fields near the corners would be terribly complicated.

We put $\mu = \mu_0$, $\epsilon = \epsilon_0$, as is approximately true for usual metal walls. The displacement current term, $-i\omega\epsilon_0$, is negligible compared to σ, even at the relatively high frequencies of our resonances. When the time variation of fields is given by a factor $e^{-i\omega t}$ as we have assumed, the correct branch of the square root in Eq. (117) is specified as follows:

$$\mathbf{E}_{\|}(\omega) = (1-i)\left|\left(\frac{\omega\mu_0}{2\sigma}\right)^{1/2}\right| \mathbf{n} \times \mathbf{H}_{\|}(\omega), \qquad \omega > 0. \tag{118}$$

This choice guarantees that the fields decay exponentially as the point of observation moves from the surface to a point within the material.

It is convenient to introduce a dimensionless complex parameter η, proportional to the square root of the resistivity; namely,

$$\eta = \frac{i}{Z_0}(1-i)\left(\frac{\omega\mu_0}{2\sigma}\right)^{1/2} = \frac{1+i}{2}\frac{\omega\delta}{c},$$

$$\delta = \left(\frac{2}{\sigma\omega\mu_0}\right)^{1/2}; \qquad |\mu| = \left[\frac{f(\mathrm{GHz})}{18\sigma(\Omega^{-1}m^{-1})}\right]^{1/2}, \qquad f = \frac{\omega}{2\pi}. \tag{119}$$

The parameter δ is the skin depth. Although η increases with frequency as $\omega^{1/2}$, it is typically small compared to 1 even at the high frequencies of our resonances (a few hundred GHz). For aluminum, $\sigma \approx 3.5 \times 10^7\ \Omega^{-1}\,\mathrm{m}^{-1}$, whereas for stainless steel, $\sigma \approx 10^6\ \Omega^{-1}\,\mathrm{m}^{-1}$. Thus for aluminum at 200 GHz, $|\eta| = 5.6 \times 10^{-4}$; for stainless steel at 600 GHz, $|\eta| = 5.8 \times 10^{-3}$.

On the cylindrical surfaces of our toroidal chamber, the boundary conditions are

$$E_\theta = \mp i\eta Z_0 H_z, \tag{120}$$

$$E_z = \pm i\eta Z_0 H_\theta, \tag{121}$$

where the upper (lower) sign is for the surface at $r = b(a)$, respectively. On the planar surfaces,

$$E_r = \pm i\eta Z_0 H_\theta, \tag{122}$$

$$E_\theta = \mp i\eta Z_0 H_r, \tag{123}$$

where the upper (lower) sign is for the surface at $z = g(-g)$, respectively.

Recalling the form of our Fourier developments [Eqs. (5), (6), and (8)], we see that Eqs. (120) and (121) might be satisfied term by term in the Fourier series. That is, E_θ and H_z are both expanded in $\sin \alpha_p(z+g)$, whereas E_z and H_θ are both expanded in $\cos \alpha_p(z+g)$. On the other hand, Eqs. (122) and (123) cannot be satisfied term by term, since fields on the left sides of the equations are expanded in sines, whereas those on the right are expanded in cosines. To accommodate the boundary conditions on planar walls, we must modify the Fourier developments.

The problem can be understood in the simplest terms by considering first the solutions of the homogeneous Maxwell equations subject to resistive-wall boundary conditions. Further, it is best to look first at solutions in which either the cylindrical walls or the planar walls are resistive, but not both at once. We thereby find that resistance of the cylindrical walls mainly effects the TE modes, whereas resistance of the planar walls mainly effects the TM modes.

We now discuss solutions of the homogeneous Maxwell equations, restricting attention to the pillbox chamber. As usual, the results are almost the same for the torus. We first treat cylindrical resistive walls, retaining infinite conductivity on the planar walls. In view of Eqs. (12), (14), (19) and (20), the conditions [Eqs. (120) and (121)] at $r = b$ imply the following equations for Fourier components:

$$\begin{aligned} &\frac{\alpha_p}{\gamma_p^2}\frac{n}{b} A_{np} J_n(\gamma_p b) + \frac{\omega}{c}\frac{Z_0}{\gamma_p} C_{np} J_n'(\gamma_p b) = \eta C_{np} J_n(\gamma_p b), \\ &A_{np} J_n(\gamma_p b) = -\eta\left[\frac{1}{\gamma_p}\frac{\omega}{c} A_{np} J_n'(\gamma_p b) + \frac{\alpha_p Z_0}{\gamma_p^2}\frac{n}{b} C_{np} J_n(\gamma_p b)\right]. \end{aligned} \tag{124}$$

These homogeneous equations for A_{np}, $Z_0 C_{np}$ have a solution only at frequencies such that their determinant $D(\omega)$ is zero. The determinant is

$$\begin{aligned} D(\omega) = &-\frac{1}{\gamma_p}\frac{\omega}{c} J_n(\gamma_p b) J_n'(\gamma_p b) \\ &+ \eta\left\{\left[1 + \left(\frac{\alpha_p n}{\gamma_p^2 b}\right)^2\right][J_n(\gamma_p b)]^2 - \left(\frac{1}{\gamma_p}\frac{\omega}{c}\right)^2 [J_n'(\gamma_p b)]^2\right\} \\ &+ \eta^2 \frac{1}{\gamma_p}\frac{\omega}{c} J_n(\gamma_p b) J_n'(\gamma_p b). \end{aligned} \tag{125}$$

When η is zero, $D(\omega)$ has zeros where $J_n(\gamma_p b) = 0$ (TM modes) and where $J_n'(\gamma_p b) = 0$ (TE modes). These zeros move into the complex plane when η is turned on.

To find the complex zero for TM modes, write

$$J_n(\gamma_p b) \approx \left[J_n'(\gamma_p b) \frac{d(\gamma_p b)}{d\omega} \right]_{\omega=\omega_r} (\omega - \omega_r), \tag{126}$$

where ω_r is the frequency of the unperturbed TM mode. Then Eq. (125) has the form

$$D(\omega) = -[J_n'(\gamma_p b)]^2 \left(\frac{1}{\gamma_p} \frac{\omega}{c} \right)^2 \frac{b}{c} \times \left\{ \omega - \omega_r + \eta \frac{c}{b} + O\left[\eta \frac{b}{c} (\omega - \omega_r)^2 \right] + O[\eta^2 (\omega - \omega_r)] \right\}. \tag{127}$$

With neglect of terms $O(\eta^2)$, the perturbed zero is at $\hat{\omega}_r = \omega_r - \eta c/b$ or

$$\hat{\omega}_r = \omega_r \left(1 - \frac{1+i}{2} \frac{\delta}{b} \right). \tag{128}$$

The corresponding Q is

$$Q = \frac{\operatorname{Re} \hat{\omega}_r}{2 |\operatorname{Im} \hat{\omega}_r|} = \frac{b}{\delta}, \tag{129}$$

(effect of cylindrical wall, TM mode).

The calculation to find the complex zero for the TE modes is much the same, if we use the Bessel equation [Eq. (86)] to eliminate the second derivative $J''(\gamma_p b)$. That is, the formula analogous to Eq. (126) is

$$J_n'(\gamma_p b) \approx \left[\left(1 - \frac{1}{z^2} \right) J_n(\gamma_p b) \frac{d(\gamma_p b)}{d\omega} \right]_{\omega=\omega_r} (\omega - \omega_r), \tag{130}$$

where, as usual, $z = \gamma_p b/n$. This yields a perturbed zero at

$$\hat{\omega}_r = \omega_r \left(1 - \frac{1+i}{2} \frac{1}{z^2 - 1} \frac{\delta}{b} \right), \tag{131}$$

and

$$Q = (z^2 - 1) \frac{b}{\delta}, \tag{132}$$

(effect of cylindrical wall, TE mode).

The quantity $z^2 - 1 = u$ is given in terms of n by Eq. (103), and is somewhat smaller than $x/R = 2(b - R)/R$. Typical values of u are given in Table I. Comparing Eqs. (129) and (132), we see that the Q due to cylindrical walls is much smaller in TE modes than in TM.

To handle resistive planar walls, we extend a method of Bart.[15] Since we need more flexibility in meeting boundary conditions, we replace the z-dependent wave functions of Eqs. (5) and (6) with

$$a_1 \sin \alpha_p (z + g) + a_2 \cos \alpha_p (z + g) \quad \text{for} \quad H_z, \tag{133}$$

$$b_1 \cos \beta_p (z + g) + b_2 \sin \beta_p (z + g) \quad \text{for} \quad E_z. \tag{134}$$

Here α_p and β_p are new wave numbers, to be determined by the boundary conditions. Since it results that α_p is very nearly equal to our old α_p of Eq. (7), we take the liberty of denoting it by the same letter. The forms Eqs. (133) and (134) are equivalent to

$$H_z^1 \cos \alpha_p z + H_z^2 \sin \alpha_p z, \tag{135}$$

$$E_z^1 \sin \beta_p z + E_z^2 \cos \beta_p z. \tag{136}$$

In the limit of infinite conductivity, only the E_z^1, H_z^1 terms survive, and only for odd p with $\alpha_p = \beta_p = \pi p/2g$ (the restriction to odd p comes from our assumption that the charge distribution is symmetric about $z = 0$). Note that the role of superscripts 1 and 2 is reversed with respect to Ref. 15, since our charge distribution excites odd p rather than the even p emphasized there.

Let us now look for a pure TM mode, a solution of the homogeneous Maxwell equations with $H_z \equiv 0$, with resistive planar walls but cylindrical walls of infinite conductivity. The wave function of E_z is

$$J_n(\hat{\gamma}_p r)(E_z^1 \sin \beta_p z + E_z^2 \cos \beta_p z), \tag{137}$$

where $\hat{\gamma}_p$ is defined by

$$\hat{\gamma}_p^2 = \left(\frac{\omega}{c}\right)^2 - \beta_p^2. \tag{138}$$

The other fields are constructed from Eq. (138) and Eqs. (11)–(14) with $H_z = 0$. It is easy to check that the full set of Maxwell's equations is satisfied separately for terms involving $\sin \beta_p z$ and $\cos \beta_p z$.

To determine β_p, substitute the above fields in the planar-wall boundary conditions [Eqs. (122) and (123)]. The boundary conditions are satisfied if

$$\begin{aligned}(x \cos x - \eta\nu \sin x)E_z^1 - (x \sin x + \eta\nu \cos x)E_z^2 = 0,\\ (x \cos x - \eta\nu \sin x)E_z^1 + (x \sin x + \eta\nu \cos x)E_z^2 = 0,\end{aligned} \tag{139}$$

$$x = \beta_p g, \qquad \nu = \frac{\omega g}{c}.$$

This homogeneous system has solutions if, and only if, its determinant D is zero:

$$D = 2(x \cos x - \eta\nu \sin x)(x \sin x + \eta\nu \cos x) = 0. \tag{140}$$

It follows that the solutions of Eq. (139) are

$$E_z^1 \text{ arbitrary}, \quad E_z^2 = 0 \quad \text{for} \quad x \cos x - \eta\nu \sin x = 0, \tag{141}$$

$$E_z^1 = 0, \quad E_z^2 \text{ arbitrary} \quad \text{for} \quad x \sin x + \eta\nu \cos x = 0. \tag{142}$$

The nonlinear equations (141) and (142) determine the wave number β_p. Since $|\eta\nu|$ is small compared to one, if the frequency is not too high, Eq. (141) has a solution x close to $\pi p/2$ for p odd, and Eq. (142) has a solution close to $\pi p/2$ for p even. By expanding the solutions in powers of $\eta\nu$, we find that one and the same function of p and $\eta\nu$ satisfies Eq. (141) for odd $p \geq 1$ and Eq. (142) for

even $p \geq 2$; namely, the complex function

$$x = x_p = \frac{\pi p}{2} - \frac{\eta\nu}{\pi p/2} - \frac{(\eta\nu)^2}{(\pi p/2)^3} + \cdots. \tag{143}$$

There is also a special solution of (Eq. 142) near zero; namely,

$$x_0 = -i(\eta\nu)^{1/2}\left(1 + \frac{1}{6}\eta\nu + \cdots\right). \tag{144}$$

The negative of each solution is also a solution, but it leads to the same wave function [Eq. (137)] and is therefore redundant.

Since $H_z = 0$, the boundary conditions on the perfectly conducting cylindrical wall are satisfied if

$$J_n(\hat{\gamma}b) = 0. \tag{145}$$

This equation is satisfied at complex ω because β_p and $\hat{\gamma}_p$ are complex. To find the complex root, expand Eq. (145) about j_{ns}, the root of J_n:

$$J_n(\hat{\gamma}_p b) \approx J_n'(j_{ns})(\hat{\gamma}_p b - j_{ns}) = 0. \tag{146}$$

Let ω_r be the frequency of the unperturbed mode, so that

$$\left(\frac{\omega_r b}{c}\right)^2 = j_{ns}^2 + \left(\frac{\pi p b}{h}\right)^2. \tag{147}$$

Then Eqs. (146) and (147) give the perturbed frequency $\hat{\omega}_r$ as

$$\begin{aligned}\left(\frac{\hat{\omega}_r b}{c}\right)^2 &= j_{ns}^2 + (\beta_p b)^2, \\ &= \left(\frac{\omega_r b}{c}\right)^2 - \left(\frac{\pi p b}{h}\right)^2 + b^2\left(\frac{\pi p}{h} - \frac{4\eta\nu}{\pi p h} + \cdots\right)^2,\end{aligned} \tag{148}$$

or, to lowest order in η,

$$\begin{aligned}\hat{\omega}_r &= \omega_r\left[1 - 4\eta\nu\left(\frac{c}{\omega_r h}\right)^2\right] \\ &= \omega_r\left[1 - (1+i)\frac{\delta}{h}\right].\end{aligned} \tag{149}$$

We have evaluated $\eta\nu$ at ω_r since the correct evaluation at $\hat{\omega}_r$ gives the same answer to lowest order in η. Thus, the quality factor is

$$Q = \frac{h}{2\delta}, \tag{150}$$

(Effect of planar walls, TM mode).

The ratio of Eq. (150) to Eq. (129) is $h/2b$, which is typically small compared to one.

The calculation for TE modes follows the same lines. In place of Eqs. (141) and

(142) we find

$$H_z^1 \text{ arbitrary}, \quad H_z^2 = 0 \quad \text{for} \quad \nu \cos x - \eta x \sin x = 0, \tag{151}$$

$$H_z^1 = 0, \quad H_z^2 \text{ arbitrary} \quad \text{for} \quad \nu \sin x + \eta x \cos x = 0, \tag{152}$$

$$x = \alpha_p g, \qquad \nu = \frac{\omega g}{c}.$$

One and the same function of p and $\eta\nu$ solves Eq. (151) for odd p and Eq. (152) for even p; namely

$$x = x_p = \frac{\pi p}{2}\left[1 - \frac{\eta}{\nu} + \left(\frac{\eta}{\nu}\right)^2 + \cdots\right]. \tag{153}$$

With

$$\hat{\gamma}_p^2 = \left(\frac{\omega}{c}\right)^2 - \alpha_p^2, \tag{154}$$

the solution of the resonance condition

$$J_n'(\hat{\gamma}_p b) = 0, \tag{155}$$

gives the following

$$\hat{\omega}_r = \omega_r\left[1 - \left(\frac{\pi pc}{\omega_r h}\right)^2 (1+i)\frac{\delta}{h}\right] \tag{156}$$

$$Q = \left(\frac{\omega_r h}{\pi pc}\right)^2 \frac{h}{2\delta}. \tag{157}$$

(Effect of planar walls, TE Modes)

The ratio of (157) to (150) is typically very large. One can ignore the effect of planar walls in lowering the Q of TE modes.

To find the combined effects of cylindrical and planar surfaces, one can, to a first approximation, add the corresponding values of Im $\hat{\omega}_r$, then take reciprocals to find Q. The result is that resistive effects of cylindrical (planar) walls are negligible in TM(TE) modes, respectively, provided that $h \ll b$. To summarize, a good approximation is

$$Q = (z^2 - 1)\frac{b}{\delta} \quad \text{(TE)}, \tag{158}$$

$$Q = \frac{h}{2\delta} \quad \text{(TM)}, \tag{159}$$

where $z^2 - 1$ is given by Eq. (103) in terms of $n = \omega R/\beta c$.

In Table I, we list the values of Q obtained from Eqs. (158) and (159) for the examples of Eq. (91), assuming that the chamber is made of aluminum, with conductivity $\sigma = 3.54 \times 10^7\ \Omega^{-1}\,\mathrm{m}^{-1}$.

It is a relatively difficult problem to find solutions of the inhomogeneous Maxwell equations with full resistive-wall boundary conditions. If only the

cylindrical walls are resistive, the inhomogeneous problems can be solved by the method of Section 2. In the case of the torus, this leads to four simultaneous equations to determine the four coefficients of Eqs. (19) and (20); for the pillbox, two simultaneous equations suffice. If the planar walls are resistive, there is an impediment to solving the inhomogeneous equations, regardless of whether the cylindrical walls are resistive. The problem is that the TE and TM fields are both excited by the sources, which means that expansions in $(\cos \alpha_p z, \sin \alpha_p z)$ get mixed with expansions in $(\cos \beta_p z, \sin \beta_p z)$. Since $\alpha_p \neq \beta_p$, the Maxwell equations with sources do not separate; i.e., they are not solved term by term in the Fourier developments. They do separate to a certain approximation, however, since α_p and β_p are both very close to $\pi p/h$.

For the numerical calculations of the following section, we take $\alpha_p = \beta_p = \pi p/h$ in deriving expressions for the impedance but finally replace $\pi p/h$ by β_p, as given by Eq. (143), in the TM terms only. [Since α_p as given by Eq. (153) is so close to $\pi p/h$, there is no reason to alter the TE terms]. The full cylindrical resistive-wall boundary conditions for the torus are imposed by solving numerically the 4×4 system to determine the coefficients of Eqs. (19) and (20). We are fairly confident that this approximate treatment is accurate, at least near the resonances and for good conductors such as copper and aluminum, because, near resonance, the solutions of the inhomogeneous equations closely resemble the eigenmodes that we have analyzed above and should have nearly the same Q. Indeed, we find that the products of $\mathcal{R}/Q$ by Q in Table I, obtained entirely from eigenmodes, agree rather well with the peak values of $\mathcal{R}$ from the full numerical calculation. The latter are shown in Figs 11. and 13. Far from resonances, where the impedance is negligible anyway, our calculation is clearly wrong since it sometimes gives small negative values of Re Z. This can be traced to a violation of charge conservation that arises from treating the nonseparable equations as though they were separable.

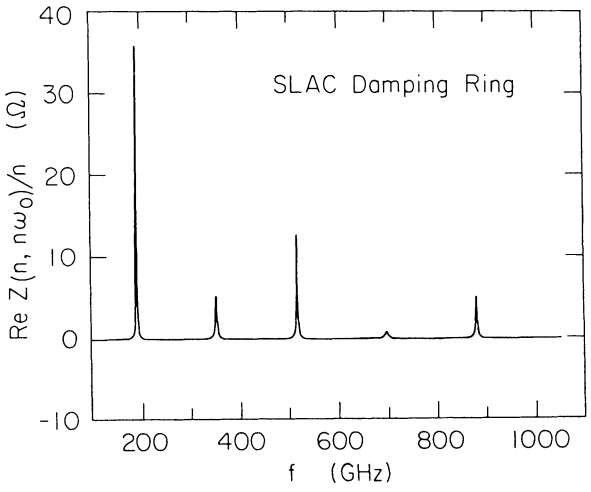

FIGURE 11 Re $Z(n, n\omega_0)/n$ versus n for SLAC damping ring.

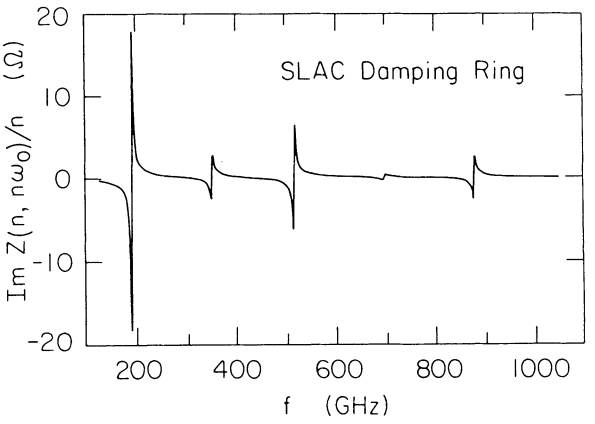

FIGURE 12 Im $Z(n, n\omega_0)/n$ versus n for SLAC damping ring.

A more accurate treatment could be devised by expanding the functions of Eq. (135) in the functions of Eq. (136), which is possible due to the completeness and orthogonality of the functions proved in Ref. 15. One would then get equations in which different values of p would be weakly coupled. A truncation of the equations to allow only a few neighboring values of p would probably lead to a satisfactory solution.

7. GRAPHS OF COUPLING IMPEDANCE AND DISCUSSION

In this section we discuss the longitudinal coupling impedance $Z(n, n\omega_0)$ as a function of n. This function is needed for stability studies based on the Vlasov

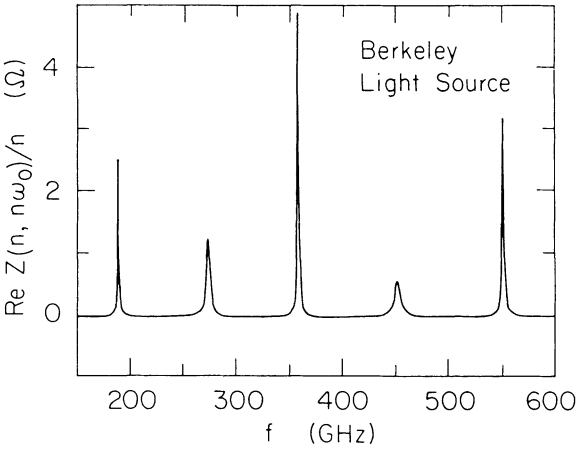

FIGURE 13 Re $Z(n, n\omega_0)/n$ versus n for Berkeley light source (ALS).

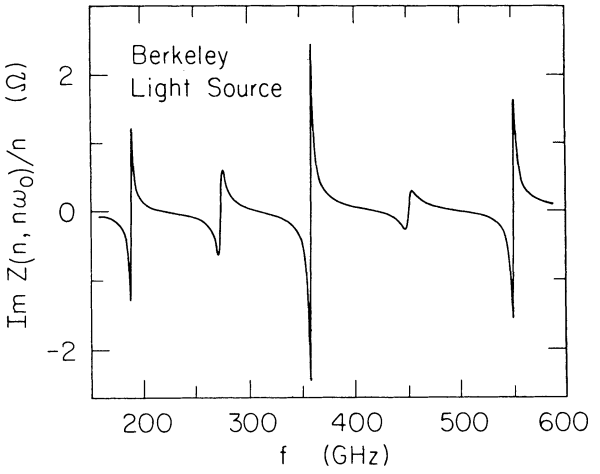

FIGURE 14 Im $Z(n, n\omega_0)/n$ versus n for Berkeley light source (ALS)

equation for bunched beams. The so-called "wake potential" $V(\omega_0\tau)$ is constructed from the same function, as a Fourier sum:

$$V(\omega_0\tau) = -2\pi R\mathscr{E}(\omega_0\tau) = \frac{\beta cq}{R}\sum_{n=-\infty}^{\infty} e^{in\omega_0\tau}Z(n, n\omega_0)\lambda_n. \tag{160}$$

Here the wake field $\mathscr{E}(\omega_0\tau)$ is the longitudinal field at an angular distance $\omega_0\tau$ ahead of a rigid bunch, averaged in time over one revolution period $2\pi/\omega_0$, and λ_n is the Fourier transform of the bunch form $\lambda(\theta)$, as in Eq. (34).

In Figs. 11 to 16, we show graphs of the real and imaginary parts of $Z(n, n\omega_0)/n$ versus n. The abscissa is labeled by the frequency f equivalent to n,

$$f = \frac{n\omega_0}{2\pi}. \tag{161}$$

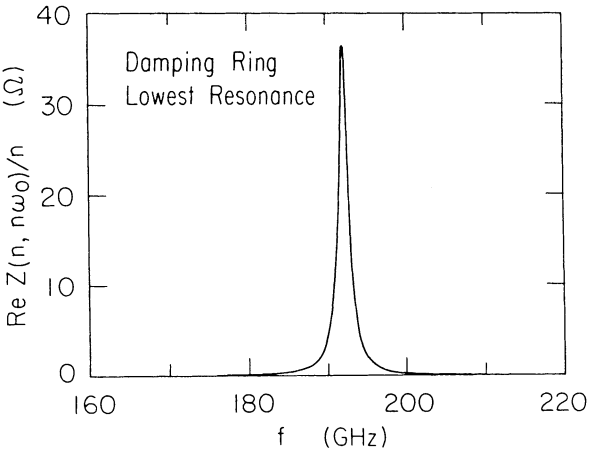

FIGURE 15 Re $Z(n, n\omega_0)/n$ versus n near lowest resonance, SLAC damping ring.

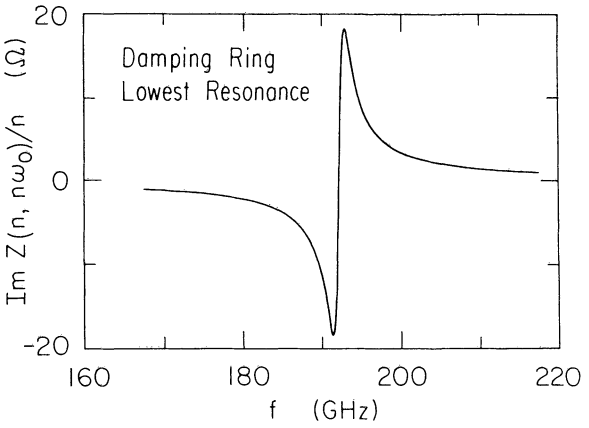

FIGURE 16 Im $Z(n, n\omega_0)/n$ versus n near lowest resonance, SLAC damping ring.

The results are for resistive toroidal chambers wih the conductivity of aluminum, $\sigma = 3.54 \times 10^7\ \Omega^{-1}\,\mathrm{m}^{-1}$, with dimensions as specified in Eq. (91). The beam is as specified in Eqs. (29) and (37), where the vertical profile $H(z) = H(-z)$ is constant over a width δh and zero elsewhere. The value of $\delta h/h$, not a critical parameter, is 0.05, and $\beta = 1$.

At frequencies lower than those shown in the graphs, the impedance is so small that it does not show up on graphs of the same scale; see Section 4. The peak of lowest frequency is a TE mode, and henceforth peaks due to TM and TE modes alternate. (Here, as throughout the paper, the designation as TE or TM refers to the axis of symmetry of the torus, not the beam direction.) The graphs were plotted from the $p = 1$ contribution alone, i.e., from the impedance due to fields excited by the lowest axial mode of the source. The contributions of higher p are negligible in the domain of frequencies plotted. At a fixed instant of time, the fields corresponding to the resonance peaks shown have tens or hundreds of thousands of oscillations in the θ direction and no, or few, oscillations in the transverse directions, z and r.

The peak values of $Z(n, n\omega_0)/n$, up to 36 Ω, are large by the standards that are usual for storage rings at lower frequencies. For instance, $|Z|/n$ for the SLAC damping ring is estimated to have a broad-band value of around 2.5 Ω up to a few GHz and is bigger than one would like. At first sight, it would seem that large impedances at frequencies of a few hundred GHz would be harmless to beam stability, since even bunches that are quite short by present standards are thought to have negligible Fourier components at such high frequencies. Thus, $Z(n, n\omega_0)\lambda_n$ in the wake potential [Eq. (160)] would be small for all n, even if Z achieves high values. This argument is not totally convincing, however, since small-scale oscillations in charge density within the bunch could give high-frequency components λ_n much bigger than those for a smooth bunch. One needs a careful examination of the bunched-beam Vlasov equation to see whether such small wiggles might build up in an unstable manner. Another point of interest is

that extremely short bunches, down to 50 μm, are being considered for future linear colliders. The short bunches would occur after the damping rings, but their coherent synchrotron radiation while going through bends could be analyzed by present methods.

There are two novel features of our impedance that may be important in stability questions. First, the peaks in Re $Z(n, n\omega_0)$ as a function of n are quite broad, with width much greater than the natural width of a single resonance. Second, the location of the peaks is a very sensitive function of the revolution frequency ω_0 (equivalently, of the trajectory radius R). These features can be understood in terms of an analytic formula for the resonant frequency as a function of n.

We return to Eq. (102), which determines the resonant frequencies. Previously, this equation was used to find poles of $Z(n, \omega)$ such that $\omega = n\omega_0$ exactly. We now apply it to find poles such that ω is merely close to $n\omega_0$. Putting

$$z^2 = \frac{[(\omega/c)^2 - \alpha_p^2]b^2}{n^2}, \tag{162}$$

and applying the approximation of Eq. (104), we can solve Eq. (102) to obtain ω as a function of n in the form

$$\omega(n) = \frac{c}{b}\left\{(\alpha_p b)^2 + n^2 + \left[3\pi\left(\frac{q}{4} + s\right)\right]^{2/3} n^{4/3}\right\}^{1/2}. \tag{163}$$

In its region of validity (large n, small $z^2 - 1$), this equation is the dispersion relation of the system. From Eq. (163) we compute the derivative

$$\begin{aligned}\frac{d\omega}{dn} &= \frac{c}{b}\left\{1 + \frac{1}{6}\left[3\pi\left(\frac{q}{4} + s\right)\right]^{2/3} n^{-2/3} + O(n^{-4/3})\right\}, \\ &\approx \frac{\beta c}{R} = \omega_0.\end{aligned} \tag{164}$$

Since $d\omega/dn$ is close to ω_0, the function $Z(n, n\omega_0)$ will not change very much when n changes by a few units. This is illustrated in Fig. 17, in which we plot Re $Z(n, n\omega_0)$ at increments of 15 in n, around the lowest peak in example (1). In this example, $\Delta n/n \approx 7.5 \times 10^{-3}$, where Δn is the full-width at half-maximum. By contrast, if we plotted Re $Z(n, \omega)$ versus ω at fixed n, we would see a much narrower peak with $\Delta\omega/\omega = 1/Q \approx 1.7 \times 10^{-5}$; here $\Delta\omega$ is the "natural line width" of the resonance.

The order of magnitude of the width Δn can be explained in terms of the linear part of $\omega(n)$ and the difference between $d\omega/dn$ and ω_0. The impedance near the resonance pole may be represented approximately as

$$Z(n, \omega) = \frac{i\zeta(n, \omega)}{\omega - \omega(n)\left(1 - \dfrac{i}{2Q}\right)}, \tag{165}$$

where ζ is real. Define n_r so that $n_r\omega_0 = \omega(n_r)$. If we expand $\omega(n)$ about n_r and

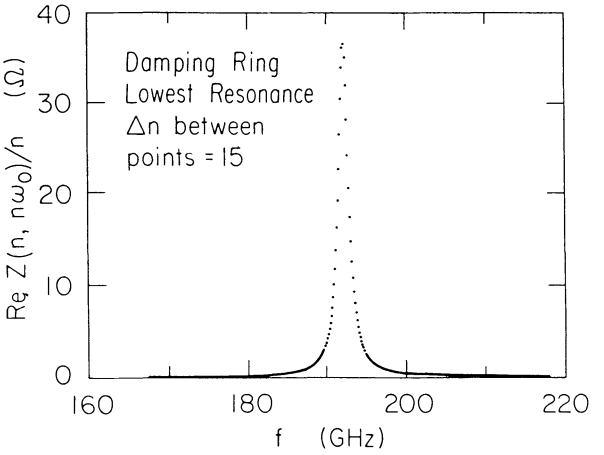

FIGURE 17 Re $Z(n, n\omega_0)/n$ versus n near lowest resonance, SLAC damping ring. The increment in n between plotted points is $\Delta n = 15$.

treat the numerator and Q as constant, we see that for $n = n_r + \Delta n/2$,

$$Z(n, n\omega_0) \approx \frac{i\zeta(n_r, n_r\omega_0)}{\left(n_r + \frac{\Delta n}{2}\right)\omega_0 - \left[\omega(n_r) + \frac{\omega'(n_r)\Delta n}{2}\right]\left(1 - \frac{i}{2Q}\right)},$$

$$= \frac{i\zeta(n_r, n_r\omega_0)}{[\omega_0 - \omega'(n_r)]\frac{\Delta n}{2} + \frac{i\omega(n_r)}{2Q}}. \tag{166}$$

We throw away the small term of order $\Delta n/Q$. Now Re $Z(n, n\omega_0)$ will reach one-half its maximum value where

$$\left|[\omega_0 - \omega'(n_r)]\frac{\Delta n}{2}\right| = \frac{\omega(n_r)}{2Q}. \tag{167}$$

Using Eq. (164) for ω' and retaining only the dominant first term, we find

$$\omega_0 - \omega'(n_r) = \frac{\beta c}{R} - \frac{c}{b} \approx \frac{wc}{2R^2}, \tag{168}$$

where $b = R + w/2$; w is the width of the chamber if the beam is centered. Thus, Eq. (166) gives the following for the full-width Δn at half-maximum:

$$\frac{\Delta n}{n} = \frac{2R}{w}\frac{1}{Q}. \tag{169}$$

For the lowest peak in example (1), we take Q from Table I, and R/w from Eq. (91) to get $\Delta n/n = 9.6 \times 10^{-3}$. This agrees well enough with the value from the exact calculation, 7.5×10^{-3}, to convince us that the linear part of $\omega(n)$ is mainly responsible for the width, Δn. The discrepancy is probably due to treating the numerator in Eq. (165) as constant.

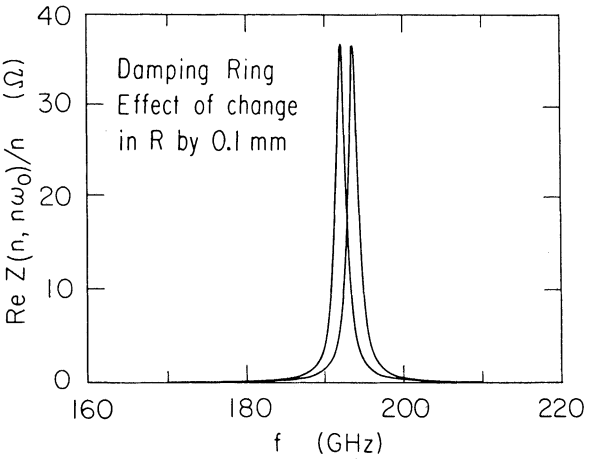

FIGURE 18 The shift in the peak of Fig. 15 when R is changed by 0.1 mm out of 5.7 m.

Although the peaks of Re $Z(n, n\omega_0)$ are broad compared to $1/Q$, they are fairly narrow compared to a typical bunch spectrum λ_n, and they are widely separated. These features should simplify the Vlasov analysis of stability.

In Fig. 18 we illustrate the sensitivity of the resonant frequencies to the value of ω_0. Changing the trajectory radius R by 0.1 mm out of 5.7 m shifts the resonance peaks by almost 2 GHz. This behavior is due to the feature noted above, that the slope of the resonance curve $\omega(n)$ at large n is just slightly smaller than the slope of the line $\omega = \omega_0 n$. The angle of intersection of the curve and the line is small, so that a small change in the slope ω_0 will produce a big change in the point of intersection, which is to say a big change in the resonant frequency that satisfies $\omega = \omega_0 n$. To find the change in frequency due to a small change in R, put $\omega = \omega_0 n$ in Eq. (163) and differentiate with respect to R. The result is

$$\frac{dn}{n} = \frac{dR}{R} \frac{\left(\frac{\beta b}{R}\right)^2}{\left(\frac{\beta b}{R}\right)^2 - 1 - \frac{2}{3}\left[\frac{3\pi(q/4+s)}{n}\right]^{2/3}}. \tag{170}$$

The factor multiplying dR/R lies in the range 350–1600 for the first few resonances of our examples.

ACKNOWLEDGEMENTS

We wish to thank R. Ruth and S. Chattopadhyay for following this work closely and making many valuable suggestions. K.-Y. Ng and L. Smith kindly pointed out errors in a first draft of this paper, and Dr. Ng verified the results in Table I, using his own formalism. Several other people were generous with encouragement, advice, and bibliographical information. In particular we thank G. Baumgartner, J. Bisognano, P. Chen, G. Decker, T. Erber, A. Faltens, and B. Zotter.

REFERENCES

1. G. A. Schott, Electromagnetic Radiation, (Cambridge University Press, Cambridge, 1912).
2. J. Schwinger, On Radiation by Electrons in a Betatron, unpublished report, 1945.
3. L. I. Schiff, *Rev. Sci. Instr.* **17,** 6 (1946).
4. L. A. Artsimovich and I. Ya. Pomeranchuk, *Zh. Eksp. Teor. Fiz.* **16,** 379 (1946).
5. J. Schwinger, *Phys. Rev.* **75,** 1912 (1949).
6. A. A. Sokolov and I. M. Ternov, Radiation from Relativistic Electrons, Amer. Inst. Phys. Translation Series, 1986.
7. J. S. Nodvick and D. S. Saxon, *Phys. Rev.* **96,** 180 (1954).
8. V. K. Neil, A Study of Some Coherent Electromagnetic Effects in High-Current Particle Accelerators, Ph.D. thesis, University of California, Berkeley, 1960; V. K. Neil, D. L. Judd, and L. J. Laslett, Rev. Sci. Instrum. **32,** 267 (1961); L. J. Laslett, V. K. Neil, and A. M. Sessler, *ibid.*, **32,** 276 (1961).
9. L. J. Laslett and W. Lewish, Evaluation of the Zeros of Cross-product Bessel Functions, Ames Laboratory Report IS-189, Iowa State University, 1960; partially reproduced in Selected Works of L. Jackson Laslett., Vol. 3, Lawrence Berkeley Laboratory Report PUB-616 (1987).
10. L. V. Iogansen and M. S. Rabinovich, *Sov. Phys. JETP* **35,** 708 (1959); *ibid.* **37,** 83 (1960); *ibid.* **11,** 856 (1960).
11. J. Vaclavik, *Czech. J. Phys.* **12,** 432 (1962).
12. A. G. Bonch-Osmolovsky, Dubna Report JINR-P9-6318, 1972.
13. A. Faltens and L. J. Laslett, *Particle Accelerators* **4,** 152 (1973); Brookhaven National Laboratory Report BNL-20550 (1975).
14. V. Brady, A. Faltens and L. J. Laslett, Lawrence Berkeley Laboratory Report LBID-536, 1981.
15. R. L. Warnock, G. R. Bart, and S. Fenster, *Particle Accelerators* **12,** 179 (1982).
16. A. Piwinski, CERN Report CERN/LEP-TH/185-43, 1985.
17. R. Talman, *Phys. Rev. Lett.* **56,** 1429 (1986).
18. M. Bassetti and D. Brandt, CERN/LEP-TH/86-04, CERN/LEP-TH/83-1; M. Bassetti, CERN/LEP-TH/86–14.
19. G. A. Decker, The Centrifugal Space Charge Force in Circular Accelerators, Ph.D. Thesis, Cornell University, 1986.
20. E. P. Lee, *Particle Acclerators* **25,** 185.
21. Handbook of Mathematical Functions, M. Abramowitz and I. A. Stegun, editors (Dover, New York, 1965).
22. F. W. J. Olver, Asymptotics and Special Functions (Academic Press, New York, 1974).
23. G. Baumgartner, Uniform Asymptotic Approximations for the Whittaker Function $M_{k,m}(z)$, Ph.D. Thesis, Illinois Institute of Technology, 1980.
24. K.-Y. Ng, *Particle Acclerators* **25,** 97.
25. K.-Y. Ng and R. Warnock, *Phys. Rev.* **D40,** 231 (1989).